Modeling the influence of resonance stabilization on the kinetics of hydrogen abstractions†

Maarten K. Sabbe,[a] Aäron G. Vandeputte,[a] Marie-Françoise Reyniers,*[a] Michel Waroquier[b] and Guy B. Marin[a]

Received 18th September 2009, Accepted 27th October 2009
First published as an Advance Article on the web 14th December 2009
DOI: 10.1039/b919479g

Resonance stabilization of the transition state is one of the key factors in modeling the kinetics of hydrogen abstraction reactions between hydrocarbons. A group additive model is developed which allows the prediction of rate coefficients for bimolecular hydrogen abstraction reactions over a broad range of hydrocarbons and hydrocarbon radicals between 300 and 1300 K. Group additive values for 50 groups are determined from rate coefficients determined using the high level CBS-QB3 *ab initio* method, corrected for tunneling and the hindered internal rotation around the transitional bond. Resonance and hyperconjugative stabilization of the transition state is accounted for by introducing 4 corrections based on the structure of the reactive moiety of the transition state. The corrections, fitted to a set of 28 reactions, are temperature-independent and reduce the mean absolute deviation on E_a to 0.7 kJ mol^{-1} and to 0.05 for log A. Tunneling contributions are accounted for by using a fourth order polynomial in the activation energy. Final validation for 19 reactions yields a mean factor of deviation between group additive prediction and *ab initio* calculation of 2.4 at 300 K and 1.8 at 1000 K. In comparison with 6 experimental rate coefficients (600–719 K), the mean factor of deviation is less than 3.

1. Introduction

Hydrogen abstraction reactions (Fig. 1) play an important role in many free-radical processes such as polymerization, combustion, pyrolysis and steam cracking of hydrocarbons. Accurate kinetic modeling of these complex processes requires a detailed reaction network that can contain hundreds of elementary hydrogen abstraction reactions. For every elementary reaction, kinetic parameters are required. Experimental determination of rate coefficients for radical reactions is complicated however, as most radicals are very unstable. Moreover, in most experimental determinations the temperature range is limited. Hence, there are only a limited number of experimentally determined kinetic parameters for hydrogen abstraction reactions available in literature. Despite the increasing computational performance, *ab initio* methods are still too demanding to determine the kinetic data for the numerous reactions in the network, particularly for larger hydrocarbons. Therefore, methods have been developed that require only a limited number of parameters to predict the kinetics for large sets of radical reactions.[1] These methods range from correlating the activation energy with the reaction enthalpy, such as Evans-Polanyi correlations and its variations,[2–4] to highly sophisticated methods based on the structure of the transition state.[5]

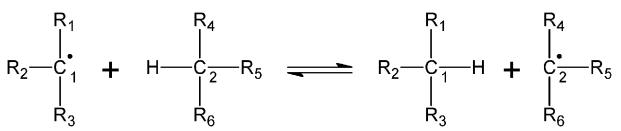

Fig. 1 Schematic representation of an H abstraction reaction.

For hydrogen abstraction reactions, the Evans-Polanyi type of correlations are generally based on a combination of valence bond theory, bond dissociation enthalpies and reaction enthalpies, such as the methods of Zavitsas,[6] Ma and Schobert,[7] and Su *et al.*[8] A disadvantage of these methods is that they are limited to the prediction of activation energies only and do not allow the prediction of pre-exponential factors. More sophisticated methods can predict both Arrhenius parameters. Most of these methods are related to Benson group additivity.[9,10] Among these are:

1. the structural group contribution method of Willems and Froment,[11,12] in which contributions added to the Arrhenius parameters of a reference reaction account for structural differences between the latter and the considered reaction.

2. methods that calculate the thermochemistry of the transition state, such as the supergroup method described by Sumathi *et al.*[13–15]

3. the Reaction Class Transition State Theory developed by Truong *et al.*[16–18]

4. the group additive (GA) method for activation energies as described by Saeys *et al.*[19,20]

Many of these methods have been developed for a limited range of hydrogen abstraction reactions. The method of Sumathi *et al.* is currently limited to H and CH_3 radicals while the reaction class transition state theory considers only

[a] *Laboratorium voor Chemische Technologie, Universiteit Gent, Krijgslaan 281 S5, B-9000 Gent, Belgium. E-mail: mariefrancoise.reyniers@ugent.be; Fax: +32 9 264 5824; Tel: +32 9 264 9655*
[b] *Center for Molecular Modeling, Universiteit Gent, Technologiepark 903, 9052 Zwijnaarde, Belgium*

† Electronic supplementary information (ESI) available: Additional data and structural details. See DOI: 10.1039/b919479g

abstractions from alkanes by H, O, OH, CHO and CH_3 radicals and from alkenes by H and OH radicals. The group additivity method as presented in previous work[20,21] can be considered as an extension of Benson's group additivity method[9,22,23] and allows prediction of the kinetic parameters for hydrogen abstractions between a broad range of hydrocarbons using a limited number of parameters. In this method, the kinetic parameters for a given reaction are written as perturbations to the kinetic parameters of the reaction methyl + methane, which is considered to be the reference reaction. The perturbations terms, *i.e.* the group additive values, thus relate to structural differences between the reaction under study and the reference reaction. Saeys *et al.*[20] reported 52 group additivity values for activation energies at 0 K. However, group additive values to predict pre-exponential factors are not yet available in literature.

The most recent work on the modeling of hydrogen abstraction reactions uses *ab initio* calculations to determine the kinetic parameters. Sumathi *et al.*[13] applied the CBS-Q complete basis set method of Ochterski *et al.*,[24] Kungwan and Truong[18] based their work upon BH&HLYP calculations and Saeys *et al.*[20] and Carstensen and Dean[25] used the CBS-QB3 method of Montgomery *et al.*[26] Numerous *ab initio* level of theory studies have been performed for hydrogen abstractions of all kinds.[27–31] Particularly for the hydrocarbon reactions in this work, the influence of the level of theory, tunneling and 1D hindered rotor treatment on the accuracy of hydrogen abstraction rate coefficients has been evaluated in a previous paper.[31] Among the evaluated methods, CBS-QB3, G3B3, MPW1PW91 and BMK with varying tunneling methods and treatment of internal rotation, best agreement with experimental data for a set of hydrogen abstractions was obtained using the CBS-QB3 method with a 1D-HR treatment of the internal rotation around the forming bond in the transition state and with Eckart corrections for tunneling effects.[32] For a test set consisting of 21 hydrogen abstractions for which accurate experimental data are available, the mean factor of deviation between experimental and calculated rate coefficients in the temperature range of 300–1000 K was found to be 6.

As reported by Saeys *et al.*,[20] the presence of resonance effects in the transition state of reactions between allylic and propargylic hydrocarbons hampers the application of the group additive method for this subclass of hydrogen abstraction reactions. To the best of our knowledge, the influence of this resonance effect on the kinetics of H-abstractions has not been reported before, since most authors consider only methyl or hydrogen radicals as abstracting radical.[13,18,25] Only the influence of resonance in the product radical on the reactivity has been discussed.[25] Clearly, an evaluation of the effect of this resonance stabilization on the kinetics is needed for an accurate modeling of the kinetics of a broad range of H-abstractions between hydrocarbons.

The aim of this work is to extend the work of Saeys *et al.*,[20] which only reports activation energies at 0 K, for both activation energies and pre-exponential factors in the temperature range 300–1300 K, including a systematic evaluation of the effects of resonance stabilization in the transition state. First, Arrhenius parameters are calculated with the CBS-QB3 composite method and, in addition to the work of Saeys *et al.*,[20] corrected for the 1D hindered rotation around the transition state bond and zero curvature tunneling according to the Eckart scheme.[31] Based on these high level *ab initio* calculations, a database of 52 group additivity values is constructed enabling the calculation of both the activation energy and the pre-exponential factor for hydrogen abstractions between a broad range of hydrocarbons (excluding polyaromatics). In this work, only abstractions by carbon-centered radicals are considered. Next, a more general approach than the one presented by Saeys[20] to account for resonance stabilization in the transition state for hydrogen transfers involving propargylic, allylic and alkylic hydrocarbons is presented. Also, a model to account for the tunneling contributions is proposed. Finally, the group additive model with corrections is validated by comparing predicted rate coefficients with *ab initio* calculated and experimental values. The temperature range covered is 300–1300 K, which encompasses most chemical applications except combustion.

2. Methodology

2.1 Computational method

Rate coefficients are calculated according to the methodology described by Vandeputte *et al.*[31] Following this procedure rate coefficients are calculated using the transition state theory (TST) in the high pressure limit:[33]

$$k_{\infty}(T) = \kappa(T)\frac{k_B T}{h}\frac{n_{\mathrm{opt},\ddagger}\, q_{\ddagger}}{n_{\mathrm{opt,A}} q_A n_{\mathrm{opt,B}} q_B} e^{-\frac{\Delta E(0\ \mathrm{K})}{RT}} \qquad (1)$$

In eqn (1) q represents the molecular partition function per unit volume, $\Delta E(0\ \mathrm{K})$ the zero point corrected electronic reaction barrier and $\kappa(T)$ the transmission coefficient accounting for quantum mechanical effects. The term n_{opt} in eqn (1) corrects for the number of optically active isomers. The activation barrier at 0 K is determined with the CBS-QB3 complete basis set method of Montgomery *et al.*[26] All *ab initio* calculations have been performed using the Gaussian 03 computational package.[34] Partition functions q are calculated using statistical thermodynamics based on a B3LYP/6-311G(2d,d,p) frequency calculation using a default scale factor of 0.99. The partition functions are evaluated using the rigid rotor and harmonic oscillator approximation assuming separability of translational, rotational, rovibrational and electronic contributions. Symmetry numbers are contained in the partition functions. In case of a symmetric hydrogen abstraction, such as for instance the reaction between methyl and methane, the transition state possesses a twofold symmetry axis that is not present along the reaction path. As pointed out by Pollak and Pechukas[35] and by Karas *et al.*,[36] any symmetry element that is present in the transition state but not along the reaction path has to be removed from the transition state partition function to avoid imposing this symmetry element on the entire reaction path. Therefore, for symmetric reactions in which a twofold symmetry axis is present in the transition state, the partition function of the transition state is divided by 2 to remove the contribution of the twofold symmetry axis.[36] Zero curvature tunneling coefficients $\kappa(T)$ were calculated using the Eckart tunneling[32] scheme as described by Vandeputte *et al.*[31] since

this method has already proven to be very successful for hydrogen abstractions.[31,37,38] In this procedure, the effective mass is approximated by the reduced mass as illustrated by Truhlar and Garrett.[39]

Within the harmonic oscillator approximation large-amplitude motions, such as internal rotations, are not treated accurately. The influence of most of the internal rotations upon the rate coefficient is limited, as the contributions of internal rotations that exist in both the reactants and the transition state largely cancel out in the rate equation (eqn (1)). For all reactions, the internal rotation about the axis formed by the breaking and forming C–H–C bond in the transition state was treated as a 1D-hindered rotation (HR) using the methodology described by Van Speybroeck *et al.*[40–43] The potential energy profiles for internal rotation were determined using a relaxed scan at the B3LYP/6-31G(d) level to which a third-order Fourier series is fitted (for exceptional sixfold symmetric rotors, a sixth order series was taken). However, for internal rotational barriers below 1 kJ mol^{-1}, the free rotor approximation was applied. Also, internal rotors in reactants and products for which the harmonic oscillator approach yielded an imaginary or extremely low frequency (<10 cm^{-1}) were treated as a free rotor.

Arrhenius parameters were fitted to the obtained rate data using linear least square regression on the Arrhenius model:

$$\ln k = \ln A - \frac{E_a}{RT} \tag{2}$$

with k sampled at intervals of 50 K between $T - 100$ and $T + 100$ K, with T the temperature of interest. The calculation of the partition functions, the tunneling corrections, the rate coefficient and the Arrhenius parameters were performed using in-house developed programs. The transition state geometries, calculation of number of single events and parameters characterising the internal rotations are given in the ESI for all reactions discussed in this paper.

In this study, the accuracy of the GA method is assessed by comparing the group additively estimated rate coefficients with *ab initio* calculated and experimental rate coefficients. As a measure for the deviation between both values the factor ρ is defined as:[21,31,44]

$$\rho = \begin{cases} \frac{k_{GA}}{k_{exp}} & \text{for } k_{GA} > k_{exp} \\ \frac{k_{exp}}{k_{GA}} & \text{for } k_{exp} > k_{GA} \end{cases} \tag{3}$$

The factor ρ is a value larger than 1 and gives a proper indication for the mutual factor of difference between both rate coefficients. It permits to calculate a mean factor of deviation for a set of reactions, $\langle\rho\rangle$, which is not possible for the ratio of both rate coefficients.

2.1 Group additivity method

In the group additive model, the rate coefficient is expressed as

$$k = \kappa n_e k_{GA} = \kappa n_e \tilde{A} \exp\left(-\frac{E_a}{RT}\right) \tag{4}$$

with κ as the tunneling coefficient, n_e the number of single events, $\tilde{A}$ the single-event pre-exponential factor and E_a the activation energy. The modeling of the Arrhenius parameters using the group additivity method has been described in detail in previous work.[20,21] In this section, attention is focused on the inclusion of resonance and hyperconjugative effects in the transition state of hydrogen transfer reactions between two allylic and/or propargylic hydrocarbons, and of hyperconjugative effects in the transition state of hydrogen transfer reactions between two alkylic hydrocarbons.

In the group additivity model, a group is defined as a polyvalent atom (coordination number $\geq$ 2) together with all of its ligands. Groups are characterized as X-$(A)_i(B)_j(C)_k(D)_l$ with X as the central atom surrounded by i A atoms, j B atoms, k C atoms and l D atoms. To describe the hydrocarbons in this work, only hydrogen and carbon atoms are required, however, but different types of carbon atoms are distinguished: C_d and C_t for a double, respectively triple bond carbon atom, $C^\bullet$ for a radical carbon and C_B for a carbon atom in a benzene ring. As shown previously,[21] the activation energy and the pre-exponential factor of a given reaction can be written as perturbations to the kinetic parameters of a reference reaction. In general, the prediction of the influence of resonance and hyperconjugative effects on a thermodynamic property is problematic using group additivity. Therefore, a formal correction, $\Delta E^{o}_{E_a,res}$, is introduced to account for their influence on the stability of the transition state of a given reaction. For the activation energy this yields:

$$E_a(T) = E_{a,ref}(T) + \sum_{i=1}^{2} \Delta GAV^{o}_{E_a}(C_i) + \sum_{i=1}^{2} \Delta GAV^{o}_{E_a}(X_i) + \sum_{i=1}^{2} \Delta GAV^{o}_{E_a}(Y_i) + \sum_{i} \Delta NNI^{o}_{i} + \Delta E^{o}_{E_a,res} \tag{5}$$

In eqn (5), the ΔGAV^{o} are related to the transition state specific groups that belong to the reactive moiety, *i.e.* the groups centered on the C, X and Y carbon atoms of Fig. 1 and pertain to structural differences between the transition state of the considered reaction and the transition state of the reference reaction. The term $\Delta E^{o}_{E_a,res}$ represents the additional stabilization of the transition state of a given reaction that cannot be included in the ΔGAV^{o}, *i.e.*, the stabilization relative to the transition state that is expected from the reactions that are used to determine the group additive values.

Saeys *et al.* have previously shown that the contributions of the group centered on the carbon atoms C_i between which the hydrogen atom is exchanged constitute the major contribution to the activation energy.[19] The substituents on the X and Y groups have only a secondary effect and can be neglected for most reactions. The non-nearest-neighbor interactions typically only influence the kinetics for reactions with strong sterical hindrance,[19,20] and can be neglected for most reactions as well. With these assumptions, the activation energy for hydrogen abstractions can be written as:

$$E_a(T) = E_{a,ref}(T) + \sum_{i=1}^{2} \Delta GAV^{o}_{E_a}(C_i) + \Delta E^{o}_{E_a,res} \tag{6}$$

The two corresponding groups are indicated as the C_1^{TS}-$(X_1)(X_2)(X_3)$ and the C_2^{TS}-$(Y_1)(Y_2)(Y_3)$ group (see Fig. 2).

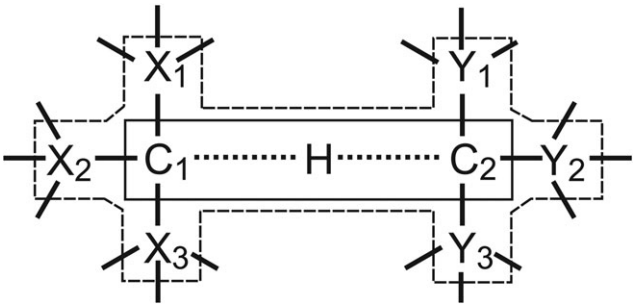

Fig. 2 Schematic representation of a H abstraction transition state. The full line indicates the central atoms of the primary contributions. The dotted line indicates which groups will contribute to the reaction kinetics if non-nearest-neighbor effects are neglected.

The subscript of the central carbon atom indicates the direction of the reaction: C_1^{TS} is the radical carbon atom that abstracts a hydrogen atom of a C_2^{TS} atom. In analogy with the work of Saeys *et al.*,[19] the H abstraction from methane by a methyl is chosen as reference reaction. Since the $\Delta GAV^{\circ}(C_1)$ are determined as the difference between the activation energy of the hydrogen abstraction by a given radical from methane and the activation energy of the reference reaction, *i.e.* the hydrogen abstraction by methyl from methane, the $\Delta GAV^{\circ}(C_1)$ include the influence of resonance and hyperconjugation due to the group centered on C_1. Similarly, the $\Delta GAV^{\circ}(C_2)$ include the influence of resonance and hyperconjugation due to the group centered on C_2. Therefore, the term $\Delta E^{\circ}_{E_a,\mathrm{res}}$ accounts for the additional resonance and hyperconjugative effects due to the simultaneous presence of groups centered on C_1 and on C_2. For instance, ΔGAV° C_1–$(C_d)(H)_2$ represents the difference in activation energy between the abstraction of a hydrogen atom from methane by methyl (R1) and by a primary allylic radical (R2).

$$CH_3^{\circ} + CH_4 \rightarrow CH_4 + CH_3^{\circ} \quad \text{(R1)}$$

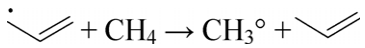

(R2)

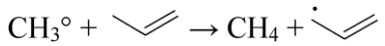

(R3)

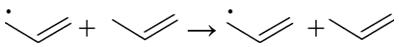

(R4)

The ΔGAV° C_2–$(C_d)(H)_2$ represents the difference in activation energy between the hydrogen abstraction by a methyl radical from methane (R1) and from propene (R3). In the hydrogen transfer reaction between two allylic moieties (R4), the term $\Delta E^{\circ}_{E_a,\mathrm{res}}$ thus accounts for the additional resonance in the transition state due to the simultaneous presence of the primary allyl group on both C_1 and C_2.

For hydrogen transfers involving a primary allylic radical, Saeys *et al.*[20] proposed a resonance correction on the group additive activation energy. The correction is function of the difference in reaction enthalpy between the studied reaction, $\Delta_r H$(298 K), and the reaction of methane with a primary allylic radical, $\Delta_r H$(298 K, methane), that is the reaction from which the ΔGAV° has been derived:

$$\Delta E_a = 0.179 \cdot |\Delta_r H(298\ \mathrm{K}) - \Delta_r H(298\ \mathrm{K}, \mathrm{methane})| \quad (7)$$

However this relation was only constructed for hydrogen abstractions from or by a primary allylic group. To calculate resonance stabilizations for reactions of other resonance-stabilized radicals, such as propargylic or benzylic groups, extra correlations should be involved. Also the additional stabilization by hyperconjugation for the reaction between a secondary allylic radical and 3-methylbut-1-ene (reaction 31, Table 2) cannot be described without the introduction of an additional correction for secondary allylic radicals. Therefore, in this work a more general model to account for resonance stabilization is proposed. Moreover, the new model should also be able to account for the resonance effects on the pre-exponential factor.

Resonance effects in the transition state can affect the entropy of the transition state, *e.g.* by influencing barriers to internal rotation, and have hence also an effect on pre-exponential factors. Therefore, similar to the activation energy (eqn (6)) a correction term $\Delta \log \tilde{A}_{\mathrm{resonance}}$ is introduced in the group additive expression for the pre-exponential factor:

$$\log \tilde{A}(T) = \log \tilde{A}_{\mathrm{ref}}(T) + \sum_{i=1}^{2} \Delta GAV^{\circ}_{\log \tilde{A}}(C_i) + \Delta \log \tilde{A}_{\mathrm{resonance}} \quad (8)$$

in which $\tilde{A}$ stands for the single-event pre-exponential factor, *i.e.*, excluding the number of single events, n_e. The relation between the single-event $\tilde{A}$ and A is:

$$\log A = \log \tilde{A} + \log n_e \quad (9)$$

n_e in eqn (9) equals the reaction path degeneracy given by (Pollak and Pechukas[35] and Coulson[45]):

$$n_e = \frac{n_{\mathrm{opt},\ddagger}}{n_{\mathrm{opt},A} n_{\mathrm{opt},B}} \frac{\sigma_A \sigma_B}{\sigma_{\ddagger}} \quad (10)$$

with σ the total symmetry number of the molecule. The total symmetry number is the product of the external symmetry number and the internal symmetry numbers. In the reaction family of hydrogen abstractions symmetric reactions can occur, as *e.g.* the reaction between a methyl radical and methane. For such reactions, an additional twofold symmetry axis is present in the transition state that is not present along the reaction paths. To avoid imposing this twofold symmetry on the entire reaction path,[35,36] the contribution of the twofold symmetry axis to the total symmetry number of the transition has to be removed. This is equivalent to multiplying the number of single events by 2 in case of a symmetric reaction with a symmetric transition state.[36]

2.3 Tunneling correction

The tunneling corrections on the *ab initio* rate coefficients are calculated using the Eckart tunneling potential, as mentioned in section 2.1. The main purpose of the group additivity method is to determine the rate coefficients for all the reactions in the network from a set of available ΔGAV° for activation energies and pre-exponential factors. However, the ΔGAV° as such do not include quantum mechanical tunneling effects. Accounting for tunneling contributions for a given reaction in the reaction network would require knowledge of the energy along the reaction path for this reaction, which, in practice, is

Table 1 Tunneling coefficients κ, pre-exponential factors [log(m^3 mol^{-1} s^{-1})], activation energies [kJmol^{-1}], rate coefficients [m^3 mol^{-1} s^{-1}] and reaction enthalpies [kJ mol^{-1}] for the training set of H-abstractions at 300 K ($k = \kappa A \exp(-E_a/RT)$, Arrhenius parameters exclude tunneling contribution)

			Forward			Reverse			
	Reaction	κ	log A	E_a	k	log A	E_a	k	$\Delta_r H^o$
1		49.07	6.171	69.7	5.4×10^{-5}	6.171	69.7	5.4×10^{-5}	0.0
2	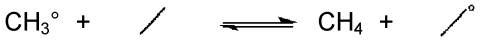	34.87	6.364	58.9	4.5×10^{-3}	5.305	74.4	7.8×10^{-7}	−15.5
3		22.69	5.880	49.0	5.0×10^{-2}	5.020	76.1	1.3×10^{-7}	−27.1
4		13.22	5.627	39.6	7.1×10^{-1}	4.917	74.0	1.4×10^{-7}	−34.4
5	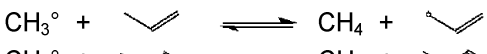	15.58	5.766	42.9	3.1×10^{-1}	6.569	118.9	1.2×10^{-13}	−75.9
6	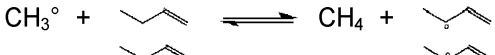	8.22	5.749	35.4	3.1×10^{0}	6.050	124.5	2.0×10^{-15}	−89.1
7		5.34	5.570	29.4	1.5×10^{1}	5.255	125.0	1.6×10^{-16}	−95.6
8	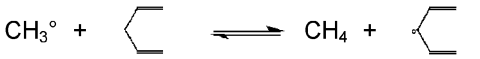	3.33	5.764	26.0	5.8×10^{1}	6.491	156.2	6.6×10^{-21}	−130.2
9		2.44	5.143	20.9	7.8×10^{1}	5.957	158.2	6.2×10^{-22}	−137.3
10		20.34	5.991	45.9	2.0×10^{-1}	6.087	104.3	1.7×10^{-11}	−58.4
11		11.63	5.826	37.9	2.0×10^{0}	5.565	108.9	4.6×10^{-13}	−71.0
12		6.86	5.501	30.3	1.2×10^{1}	5.109	110.7	4.7×10^{-14}	−80.4
13		5.07	5.787	27.8	4.5×10^{1}	6.066	133.6	3.3×10^{-17}	−105.8
14	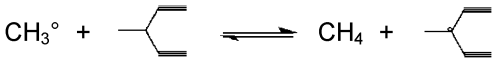	3.39	5.457	22.0	1.4×10^{2}	5.532	137.8	1.2×10^{-18}	−115.8
15	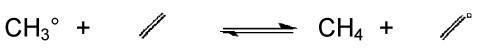	30.93	6.244	69.3	4.6×10^{-5}	5.925	47.5	1.4×10^{-1}	21.8
16	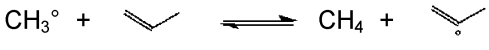	28.63	5.668	60.0	4.7×10^{-4}	5.728	51.0	2.0×10^{-2}	9.0
17		36.44	5.976	59.8	1.3×10^{-3}	5.681	80.7	1.6×10^{-7}	−20.9
18	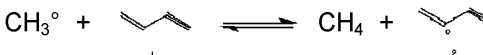	22.40	5.533	49.0	2.3×10^{-2}	5.059	68.7	2.8×10^{-6}	−19.7
19		16.46	5.522	49.5	1.3×10^{-2}	5.947	110.2	9.4×10^{-13}	−60.7
20		9.05	5.589	41.5	2.1×10^{-1}	5.871	112.0	2.1×10^{-13}	−70.4
21	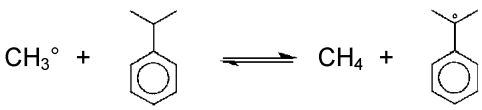	7.31	5.177	36.1	5.6×10^{-1}	4.576	109.4	2.4×10^{-14}	−73.3
22		15.62	6.430	75.9	2.6×10^{-6}	5.839	33.9	1.3×10^{1}	42.0
23	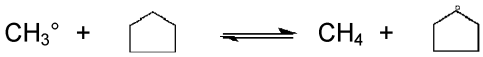	19.14	5.011	44.4	3.7×10^{-2}	5.951	81.6	1.1×10^{-7}	−37.2
24	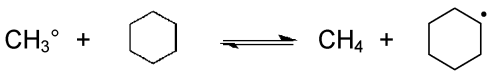	24.17	6.319	49.0	1.5×10^{-1}	5.407	73.8	8.6×10^{-7}	−24.9
25		14.50	5.326	38.9	5.1×10^{-1}	4.906	71.2	4.6×10^{-7}	−32.3
26	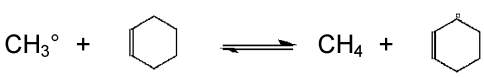	7.64	6.042	32.2	2.1×10^{1}	5.919	123.7	1.9×10^{-15}	−91.5

not available during the application of the group additive method. Therefore, a method allowing to correct the group additively calculated rate coefficients for quantum mechanical tunneling effects that avoids explicit calculation of the tunneling coefficients for all the reactions present in the reaction network is proposed.

The method developed to correct the GAV-calculated rate coefficient for tunneling is based on the idea that reactions belonging to the same reaction class have similarities in the potential energy surface along the reaction path.[46] This feature is also applied in the reaction class transition state theory, developed by Truong,[46] to transfer high-level tunneling calculations performed on the small reactions of the reaction class to the tunneling contributions of the larger reactions. The tunneling coefficient for a given reaction in the class is determined by multiplying the temperature dependent tunneling

Table 2 Tunneling coefficients κ, pre-exponential factors [log(m^3 mol^{-1} s^{-1})], activation energies [kJ mol^{-1}], rate coefficients [m^3 mol^{-1} s^{-1}] and reaction enthalpies [kJ mol^{-1}] for the set of H-abstractions to evaluate resonance stabilization at 300 K ($k = \kappa A \exp(-E_a/RT)$, Arrhenius parameters exclude tunneling contribution)

			Forward			Reverse			
	Reaction	κ	log A	E_a	k	log A	E_a	k	$\Delta_r H^o$
27	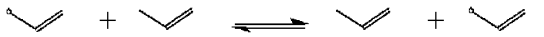	144.9	5.682	81.7	4.1×10^{-7}	5.682	81.7	4.1×10^{-7}	0.0
28	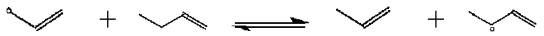	102.3	5.547	71.2	1.4×10^{-5}	5.046	84.3	2.3×10^{-8}	−13.1
29	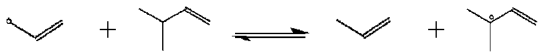	56.1	5.407	60.6	4.0×10^{-4}	4.290	80.3	1.1×10^{-8}	−19.7
30	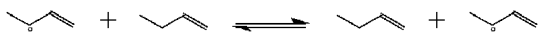	78.4	4.973	71.4	2.8×10^{-6}	4.973	71.4	2.8×10^{-6}	0.0
31	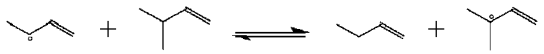	57.5	4.604	63.5	2.1×10^{-5}	3.988	70.0	3.6×10^{-7}	-6.6
32	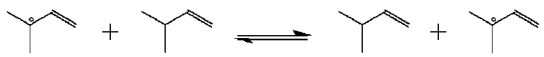	44.6	3.615	60.3	5.9×10^{-6}	3.615	60.3	5.9×10^{-6}	0.0
33	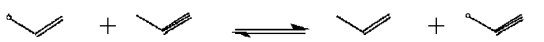	94.5	6.304	86.7	1.5×10^{-7}	5.598	69.2	3.4×10^{-5}	17.6
34	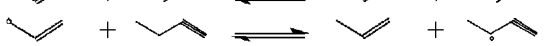	78.1	5.756	75.1	3.7×10^{-6}	4.693	70.2	2.3×10^{-6}	4.9
35	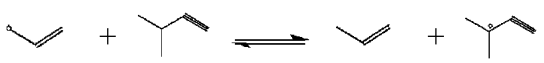	56.8	5.636	64.5	1.5×10^{-4}	4.442	69.0	1.5×10^{-6}	−4.5
36	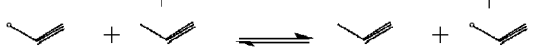	92.1	5.853	74.9	6.0×10^{-6}	5.853	74.9	6.0×10^{-6}	0.0
37	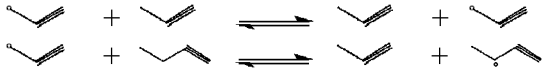	65.3	5.621	63.0	2.9×10^{-4}	5.264	75.7	8.0×10^{-7}	−12.6
38	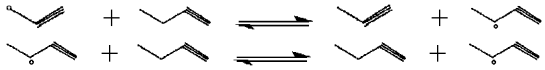	55.3	4.688	63.7	2.2×10^{-5}	4.688	63.7	2.2×10^{-5}	0.0
39	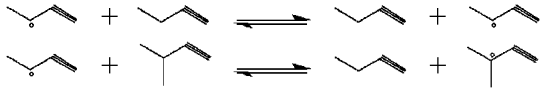	38.8	4.551	52.1	1.2×10^{-3}	4.420	61.5	2.0×10^{-5}	−9.4
40	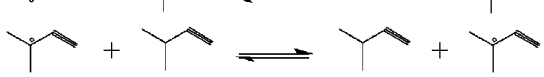	32.7	3.897	50.3	4.4×10^{-4}	3.897	50.3	4.4×10^{-4}	0.0
41	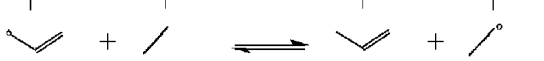	25.1	6.699	104.5	8.1×10^{-11}	4.837	44.0	3.7×10^{-2}	60.4
42		27.7	6.197	90.6	7.3×10^{-9}	4.535	41.8	5.1×10^{-2}	48.8
43	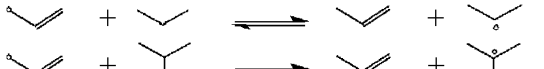	23.8	5.894	79.2	3.0×10^{-7}	4.381	37.7	1.6×10^{-1}	41.6
44	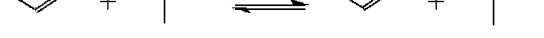	19.4	5.546	97.0	8.7×10^{-11}	4.385	35.1	3.7×10^{-1}	61.9
45	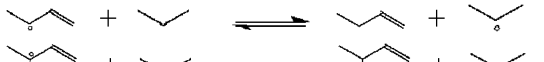	12.0	4.736	96.5	1.0×10^{-11}	4.191	28.0	2.5	68.5
46		11.1	4.139	69.7	1.1×10^{-7}	3.821	23.6	5.7	46.1
47	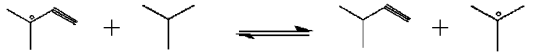	37.2	4.602	54.7	4.4×10^{-4}	4.602	54.7	4.4×10^{-4}	0.0
48		26.1	3.898	40.8	1.7×10^{-2}	3.898	40.8	1.7×10^{-2}	0.0
49	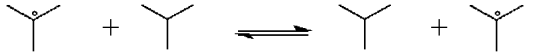	20.0	5.992	46.5	1.6×10^{-1}	5.992	46.5	1.6×10^{-1}	0.0
50	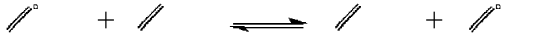	4.3	5.472	21.6	2.2×10^{2}	6.594	119.4	2.7×10^{-14}	−97.8
51	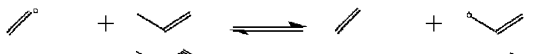	1.8	5.176	10.6	3.9×10^{3}	5.104	112.9	5.1×10^{-15}	−102.3
52	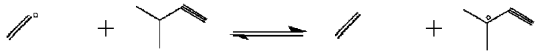	13.3	6.151	36.5	8.1	5.412	73.9	4.6×10^{-7}	−37.4
53	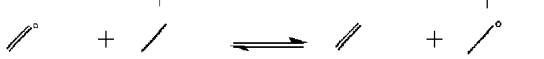	6.8	5.682	27.0	6.6×10^{1}	5.142	75.9	5.7×10^{-8}	−48.9
54	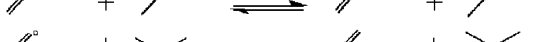	8.9	6.407	108.9	2.5×10^{-12}	5.310	53.8	7.7×10^{-4}	55.1

coefficient of the reference reaction with a relative, temperature dependent, function. Kungwan and Truong successfully applied this approach to predict rates for hydrogen abstractions from alkanes and alkenes by hydrogen and methyl radicals.[17,18,47,48]

In this work a more pragmatic approach is followed to obtain the tunneling contribution for a given hydrogen abstraction reaction based on properties that are easily accessible during the group additive prediction. In practice, the main factors controlling tunneling in the zero-curvature approximation, *i.e.*, the net electronic tunneling barrier and the imaginary frequency in the transition state, are not accessible during the application of the group additive model for rate prediction. However, the net electronic barrier, which is the section of the reaction barrier through which tunneling is possible, *i.e.*, without endothermic contributions, corresponds to the electronic barrier of the exothermic direction of the reaction. The Arrhenius activation energy for the exothermic reaction, which can be predicted using group additivity, thus provides a good measure for the electronic tunneling barrier. Within this approximation, the tunneling contribution to the rate coefficient of a reaction in the family can be expressed as a function of the temperature and the activation energy of the exothermic direction of the reaction, $\kappa(T,E_{a,exo})$. Therefore, in this work, a generalized correction for tunneling, $\kappa(T,E_{a,exo})$, is derived by fitting to the Eckart tunneling coefficients of the reactions mentioned in Tables 1 and 2.

3. Results and discussion

3.1 Rate coefficients and Arrhenius parameters

The tunneling coefficients, Arrhenius parameters and rate coefficients for the set of 26 hydrogen abstraction reactions by methyl radicals, from which the group additive values are determined, are given in Table 1 (300 K). The 28 reactions from which the influence of resonance stabilization in the transition state is evaluated are tabulated in Table 2. The influence of resonance effects on the activation energy and pre-exponential factors due to the simultaneous presence of groups centered on C_1 and C_2 has been evaluated for hydrogen abstractions between species with a varying degree of resonance and hyperconjugative stabilization (see Table 2). The species considered include vinyl radicals, which are stabilized by neither resonance nor hyperconjugation effects, resonance-stabilized primary allyl and propargyl radicals, methyl substituted allyl and propargyl radicals, which are stabilized by resonance as well as by hyperconjugation, and alkylic radicals with various degrees of hyperconjugative stabilization. Kinetic data at 600 and 1000 K are available in The ESI, Tables S1 and S2, respectively.† The transition state geometries are given in the ESI for all reactions. In contrast to Carstensen and Dean,[25] all geometries agreed to the expected geometry.[49]

Most of the hydrogen abstraction reactions involving methyl radicals (Table 1) are exothermic since in most cases the formed radicals are more stable than the methyl radical. At 300 K, the rate coefficients range between 10^{-22} and 10^{4} m^3 mol^{-1} s^{-1}. The slowest reactions are abstractions by the most resonance-stabilized radicals, such as diallylic radicals (reverse reactions 8–9) and dipropargylic radicals (reverse reactions 13–14), while the fastest reactions are obviously the corresponding reverse reactions. The internal rotations about the transitional C–H–C bond have a significant contribution to the rates, particularly for abstractions by methyl radicals; due to the small size of the methyl radical all rotations have barriers below 1 kJ mol^{-1} and are treated as a free rotor. Accounting for the internal rotation decreases rate coefficients up to a factor of 10 for the reactions with the lowest HO-rovibrational frequencies in the transition state. The low barriers are indicative of the small effect of steric interactions for H-abstractions, and the rotational barriers are, even for reactions with radicals larger than methyl (Table 2), generally limited to a few kJ mol^{-1}, with exceptions up to 12 kJ mol^{-1} for the reaction of a propargyl radical with propyne (reaction 36).

The tunneling coefficients (Table 1–2) range between 1.8 and 150. The Arrhenius parameters reported in Table 1–2 have been determined from rate coefficients without tunneling contributions. For the abstractions by methyl (Table 1), the pre-exponential factors span a rather narrow range with $\log(A/m^3\ mol^{-1}\ s^{-1})$ varying between 5.0 and 6.5. The largest values pertain to abstractions leading to less stable radicals, such as vinylic and phenyl radicals (reactions 15 and 22) while the lowest values are related to the formation of the resonance-stabilized radicals, such as diallylic, dipropargylic and benzylic radicals. The limited dependence of the pre-exponential factors to substitution at the attacked site is in agreement with the findings of Carstensen and Dean.[25] For the abstractions by other radicals, the values for log A show a broader variation and range from 3.6 (reaction 32) to 6.7 (reaction 41).

The activation energies vary over a very broad range and mainly depend on the relative stabilities of the reactant and product radical. For the abstractions by methyl, an obvious decrease in activation energy is observed for stronger resonance-stabilization in the product radical in agreement with other work,[25] with the activation energies ranging from 20 kJ mol^{-1}, for the formation of the strongly stabilized radicals of reactions 9 and 14, to 76 kJ mol^{-1} for the formation of the phenyl radical (reaction 22). For most of the hydrogen abstractions from methane, the activation energies are, due to the their endothermicity, larger and amount up to 158 kJ mol^{-1} for the abstraction by the resonance stabilized 3-methylpenta-1,4-dien-3-yl (reverse reaction 9). For the reactions in Table 2, the activation energy varies between 10 and 120 kJ mol^{-1}.

As illustrated in Fig. 3, an accurate prediction of the activation energy for the reactions mentioned in Tables 1 and 2 using a simple Evans-Polanyi correlation can be expected to be problematic.

3.2 Resonance interactions

In this section, the presence of resonance and hyperconjugative interactions in the transition state is discussed. As mentioned above, corrections are necessary to account for these effects due to the simultaneous presence of groups centered on C_1 and on C_2, *i.e.* cross-resonance and cross-hyperconjugation. The influence of resonance effects on the Arrhenius parameters due to the simultaneous presence of groups centered on C_1 and C_2

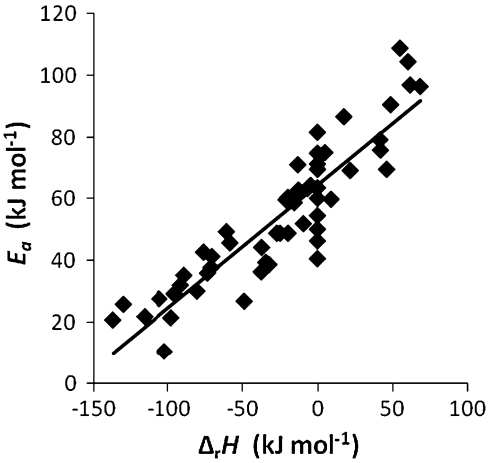

Fig. 3 Evans-Polanyi plot for the reactions from Tables 1 and 2, with linear Evans-Polanyi correlation shown ($E_a = 0.4\Delta_r H + 64.8$) (298 K).

has been evaluated for hydrogen abstractions between species with various types of resonance and hyperconjugative stabilization. These involve resonance stabilization between allylic and propargylic fragments, and hyperconjugative stabilization between an allylic/propargylic fragment and a β C–H bond (see Table 2 for the full set of reactions). Note that hyperconjugative effects involving β C–C bonds are not included in the available set of reactions.

The presence of resonance stabilization can be clearly illustrated by comparing the Mulliken spin densities for the transition states of the allyl + methane (reaction 5 of Table 1) and the allyl + propene (reaction 27 of Table 2) in Fig. 4. Graphical representations of the HOMO of the transition states for these reactions, and for the other reactions discussed in this section, can be found in the ESI (Fig. S2).† For reaction 5, the radical is delocalized over the methyl p orbital and the p orbitals of the allyl system. From this reaction the

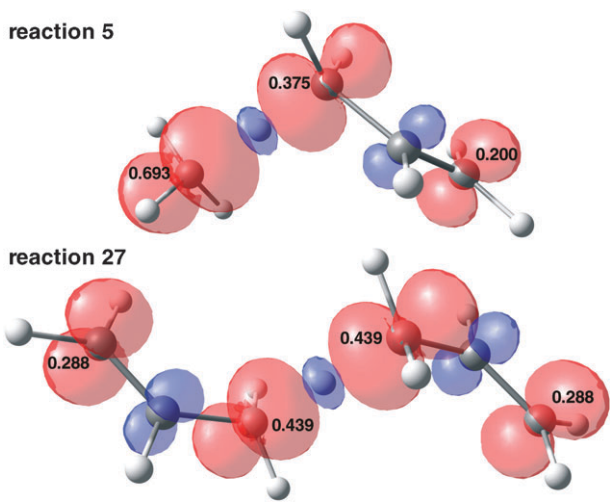

Fig. 4 Spin density plots illustrating the resonance stabilization of the transition state for reactions of allylic radicals, with indication of the most important Mulliken atomic spin densities. Top: Allyl + methane (reaction 5), Bottom: Allyl + propene (reaction 27) (B3LYP/6-311G(d,p), 0.006 isosurfaces).

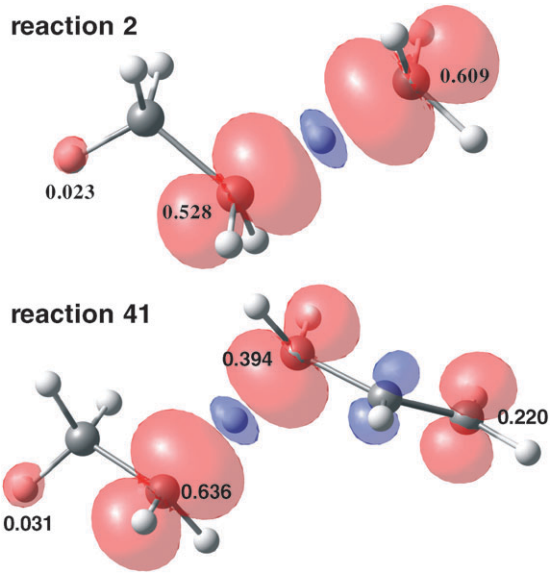

Fig. 5 Spin density plots illustrating the hyperconjugative stabilization of the transition state for reactions between allylic radicals and alkanes, with indication of the most important Mulliken atomic spin densities. Top: methyl + ethane (reaction 2), Bottom: allyl + ethane (reaction 41) (B3LYP/6-311G(d,p), 0.006 isosurfaces).

contributions to account for an allylic fragment centered on C_1 or C_2 are derived. Hence, these contributions (ΔGAV^o) account for the radical delocalization in the allyl fragment centered either on C_1 or on C_2. In reaction 27, the simultaneous presence of allyl fragments on both the C_1 and C_2 atom provides p orbitals available for electron delocalization that extend beyond the local entity described by the allylic fragment, as illustrated by the spin densities in Fig. 4. Therefore, the stabilization of the transition state of reaction 27 resulting from the electronic coupling between the two allyl fragments on C_1 and C_2 cannot be accounted for by contributions taken from reaction 5 since these cross conjugation effects are not included. As illustrated in Fig. 5 and 6, similar cross conjugation effects can be expected for other radicals stabilized by resonance or hyperconjugation. Only additivity methods using entities that encompass the two radical centers of the transition state, as *e.g.* the supergroups introduced by Sumathi *et al.*,[13] are able to include these cross effects without requiring additional corrections. However, the use of supergroups would require the introduction of a supergroup for every possible combination of allylic, propargylic or benzylic groups, leading to a combinatorial increase in the number of supergroups needed. Therefore, a correction method based on the various types of electronic cross-interaction between the two substituents seems to be more reasonable, as this significantly reduces the number of required parameters.

The following combinations have been considered: (i) $\pi_{=}$–$\pi_{=}$, (ii) $\pi_{=}$–$\pi_{\equiv}$, (iii) $\pi_{\equiv}$–$\pi_{\equiv}$, (iv) π–$\sigma_{\beta C-H}$ and (v) $\sigma_{\beta C-H}$–$\sigma_{\beta C-H}$ cross interactions. The first type of cross conjugation between two allylic fragments, $\pi_{=}$–$\pi_{=}$, is exemplified by the allyl + propene reaction. The second combination is the $\pi_{=}$–$\pi_{\equiv}$ cross resonance conjugation between an allylic and a propargylic fragment in the transition state, which is a cross-resonance effect akin to the first type of

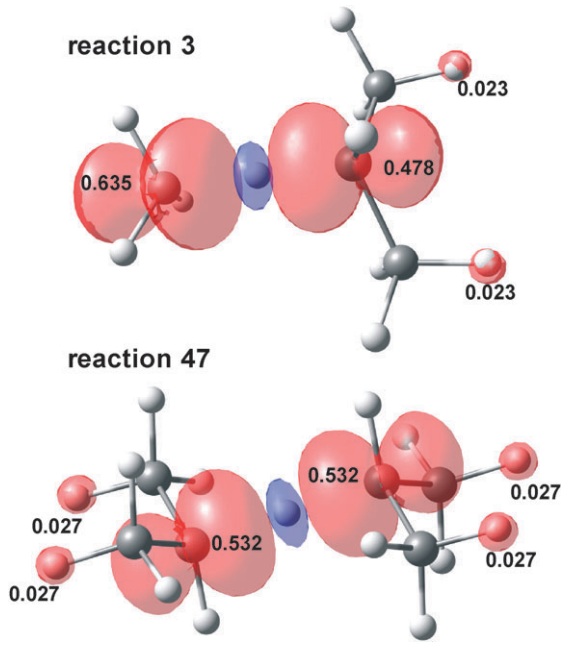

Fig. 6 Spin density plots illustrating the hyperconjugative stabilization of the transition state for reactions between an *iso*-propyl radical and propane, with indication of the most important Mulliken atomic spin densities. Top: iso-propyl + methane (reaction 3), bottom: iso-propyl and propane (reaction 47) (B3LYP/6-311G(d,p), 0.006 isosurfaces).

$\pi_{=}$–$\pi_{=}$ cross conjugation. The third combination, representing the stabilizing interaction in transition states between propargylic fragments, $\pi_{\equiv}$–$\pi_{\equiv}$, shows a similar resonance pattern. The fourth combination π–$\sigma_{\beta C-H}$ describes the cross stabilization due to resonance stabilization in one fragment and hyperconjugative stabilization in the other fragment. The smallest possible reaction with this type of cross-stabilization is the reaction of an allyl radical with ethane. The Mulliken spin density plots of Fig. 5 illustrate the cross-resonance-hyperconjugative effect in the transition states of the reaction of the methyl and allyl radical with ethane. The effect of π–$\sigma_{\beta C-H}$ interaction appears to be small, but since the ethyl radical has only a single hyperconjugation possibility in contrast to multiply alkyl substituted radicals, the contribution is expected to be significant for larger substituted radicals. The distribution of the spin density in the transition state is different from the spin densities in the training set reactions, which are the reactions of an ethyl and allyl radical with methane. This difference is mainly due to the difference in the location of the transition state. For the reaction between the methyl radical and ethane, the transition state is more reactant like and the spin density is mainly located on C_1, the methyl carbon atom (see Fig. 5). In contrast, for the reaction between the resonance stabilized allyl radical and ethane, the transition state is more product like and the spin density is mainly located on the C_2 carbon atom of ethane resulting in an increased hyperconjugative overlap with the β C–H bond (see Fig. 5). As illustrated in Fig. 6 for the reaction of and *iso*-propyl radical with propane, cross-hyperconjugative stabilization of the transition state also occurs for reactions between substituted alkyl radicals. The spin density plot clearly shows the redistribution of the spin density indicative of cross-hyperconjugative stabilization. Other examples of this type of stabilization are given in the ESI. The magnitude of the effect of the $\sigma_{\beta C-H}$–$\sigma_{\beta C-H}$ interaction can be expected to be small, but might contribute significantly for reactions between multiply substituted alkyl radicals.

Clearly, stabilizing cross-conjugation and cross-hyperconjugation interactions that act beyond the local groups are present in the transition state. Accurate modeling of the kinetics of these hydrogen abstraction reactions requires that the interactions are explicitly accounted for. Therefore, a model is proposed that takes a stabilizing correction into account for every occurrence of a $\pi_{=}$–$\pi_{=}$, $\pi_{=}$–$\pi_{\equiv}$, $\pi_{\equiv}$–$\pi_{\equiv}$, π–$\sigma_{\beta C-H}$ and $\sigma_{\beta C-H}$–$\sigma_{\beta C-H}$ interaction. This stabilization correction is added to the group additive prediction of E_a and log A to obtain a proper prediction of the Arrhenius parameters. As will be discussed later (see section 3.3.2 on resonance corrections), the $\pi_{=}$–$\pi_{=}$ and $\pi_{=}$–$\pi_{\equiv}$ correction can be grouped together in the $\pi_{=}$–$\pi_{=/\equiv}$ correction.

The number of corrections can be obtained by counting the number of cross interactions between the groups centered on C_1 and C_2. The number of corrections required to account for cross-π-conjugation of the type $\pi_{=}$–$\pi_{=/\equiv}$ (correction 1) can be obtained by multiplying the number of allyl systems on one fragment with the number of allyl/propargylic systems on the other fragment. For instance, the reaction of an allyl radical with propene or propyne requires 1 $\pi_{=}$–$\pi_{=/\equiv}$ correction while the reaction of the penta-1,4-dien-3-yl radical with propene requires 2 such corrections. Similarly, the number of corrections required to account for cross conjugation between two propargylic π-systems (correction 2, $\pi_{\equiv}$–$\pi_{\equiv}$) is obtained as the number of interactions between the propargylic structures on C_1 and those on C_2. For instance, the reaction between a propargyl radical with propyne requires the use of 1 $\pi_{\equiv}$–$\pi_{\equiv}$ correction. The number of cross-π-hyperconjugative interactions π–$\sigma_{\beta C-H}$ (correction 3) amounts to the number of interactions between unsaturated bonds in one fragment and alkyl substituents on the radical center of the other fragment and can be obtained as

$$n(\pi\text{–}\sigma_{\beta C-H}) = n_{\pi 1}n_{\sigma 2} + n_{\pi 2}n_{\sigma 1}$$

with $n_{\pi 1}$ the number of π systems in resonance with the radical on C_1, $n_{\sigma 2}$ the number of alkyl substituents on the C_2 radical atom, *etc.* For instance, a single cross-π-hyperconjugative correction is required for the reaction between an allyl radical and ethane, as well as for the reaction between a but-1-en-3-yl radical and propene, while two π–$\sigma_{\beta C-H}$ corrections are needed for the reaction of an allyl radical with propane forming 2-propyl, as well as for the reaction of a penta-1,4-dien-3-yl radical with ethane. The number of corrections required for cross-hyperconjugation (correction 4, $\sigma_{\beta C-H}$–$\sigma_{\beta C-H}$) is obtained as the number of interactions between the alkyl substituents on the first radical center with those on the second radical center and can be obtained by multiplying the number of alkyl substituents at C_1 with the number of alkyl substituents at C_2. For instance, a single cross-hyperconjugation correction is required for the reaction of ethyl with ethane and for the reaction between the but-1-en-3-yl radical and ethane, while

four $\sigma_{\beta C-H}$–$\sigma_{\beta C-H}$ corrections are needed for the symmetric reaction of 2-propyl with propane.

3.3 Group additive model

3.3.1 Group additive values. The group additive values ΔGAV^{o} required to describe the kinetics of hydrogen transfer between a broad range of hydrocarbons, are derived from the Arrhenius parameters of Table 1. Each ΔGAV^{o} is determined from a single reaction. The applied number of single events can be retrieved in Table S3 of the ESI.

The group additive values at 300 and 1000 K are presented in Table 3, and the temperature-dependent Arrhenius parameters for the reference reaction are given in Table 4. For the abstracting radical C_1, the group additive values can be directly related to the stability of the abstracting radical. The ΔGAV^{o} for activation energies increase with increasing stability of the abstracting radical, with as largest influences +88.5 kJ mol^{-1} for the $\Delta GAV^{o}_{E_a}$ of the diallylic C_1–$(C_d)_2$(C) group and −35.8 kJ mol^{-1} for the $\Delta GAV^{o}_{E_a}$ of the unstable phenyl $C_{1,B}$-group. For pre-exponential factors the values range between −1.294 for the C_1–$(C_B)(C)_2$ group and +0.320 for the C_1–$(C_d)_2$(H) group. There is no correlation with the ΔGAV^{o} for the activation energy. In general, the $\Delta GAV^{o}_{\log A}$ decrease with increasing methyl substitution on the abstracting radical. For the formed radical C_2, the $\Delta GAV^{o}_{E_a}$

Table 4 Single-event Arrhenius parameters for the reference reaction ($CH_3^{\bullet}$ + CH_4 hydrogen abstraction) in the temperature range from 300 to 1300 K

T/K	log A/m^3 mol^{-1} s^{-1}	E_a/kJ mol^{-1}
300	5.267	69.7
400	5.453	70.9
500	5.662	72.6
600	5.863	74.7
700	6.050	77.0
800	6.219	79.5
900	6.371	81.9
1000	6.509	84.4
1100	6.633	86.9
1200	6.746	89.4
1300	6.849	91.9

Table 3 Standard group additivity values for the group additivity method at 300 K and 1000 K (HR without tunneling contributions, m^3 mol^{-1} s^{-1} and kJ mol^{-1})

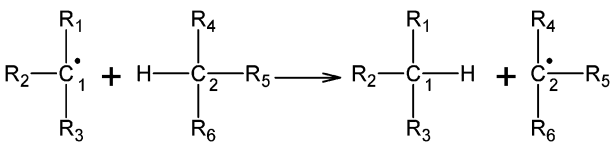

		300K				1000K			
		C_1 contribution		C_2 contribution		C_1 contribution		C_2 contribution	
No.	Group	$\Delta GAV^{o}_{\log A}$	$\Delta GAV^{o}_{E_a}$	$\Delta GAV^{o}_{\log A}$	$\Delta GAV^{o}_{E_a}$	$\Delta GAV^{o}_{\log A}$	$\Delta GAV^{o}_{E_a}$	$\Delta GAV^{o}_{\log A}$	$\Delta GAV^{o}_{E_a}$
	Reference reaction: $CH_3^{\bullet} + CH_4$	5.267	69.7	5.267	69.7	6.509	84.4	6.509	84.4
1	C_i–(C)(H)$_2$	−0.866	+4.7	+0.017	−10.8	−0.790	+5.4	+0.071	−10.4
2	C_i–$(C)_2$(H)	−0.850	+6.5	+0.010	−20.6	−0.682	+8.0	+0.101	−20.0
3	C_i–$(C)_3$	−0.953	+4.3	+0.059	−30.1	−0.628	+7.3	+0.187	−29.1
4	C_i–(C_d)(H)$_2$	+0.097	+49.2	−0.581	−26.8	+0.334	+51.3	−0.535	−26.5
5	C_i–(C_d)(C)(H)	−0.121	+54.8	−0.121	−34.3	+0.144	+57.2	−0.025	−33.5
6	C_i–$(C_d)(C)_2$	−0.916	+55.3	−0.300	−40.3	−0.618	+58.1	−0.203	−39.6
7	C_i–$(C_d)_2$(H)	+0.320	+86.5	−0.105	−43.7	+0.658	+89.5	+0.007	−42.9
8	C_i–$(C_d)_2(C)$	−0.213	+88.5	−0.425	−48.8	+0.419	+94.8	−0.339	−48.2
9	C_i–(C_t)(H)$_2$	−0.083	+34.6	−0.055	−23.8	+0.059	+35.9	−0.010	−23.5
10	C_i–(C_t)(C)(H)	−0.606	+39.2	−0.044	−31.8	−0.389	+41.2	+0.046	−31.1
11	C_i–$(C_t)(C)_2$	−1.061	+41.0	−0.067	−39.4	−0.772	+43.7	+0.049	−38.6
12	C_i–$(C_t)_2$(H)	−0.105	+63.9	−0.082	−41.9	+0.181	+66.5	−0.002	−41.3
13	C_i–$(C_t)_2(C)$	−0.639	+68.1	−0.111	−47.7	−0.025	+74.3	−0.002	−46.9
14	$C_{i,d}$–(H)	+0.055	−22.2	+0.074	−0.4	+0.288	−20.1	+0.132	+0.0
15	$C_{i,d}$–(C)	−0.141	−18.7	+0.100	−9.7	+0.158	−15.9	+0.176	−9.2
16	$C_{i,d}$–(C_d)	−0.188	+11.0	+0.106	−9.9	−0.010	+12.6	+0.186	−9.4
17	$C_{i,d}$–(C_t)	−0.810	−1.0	−0.035	−20.7	−0.702	+0.1	+0.030	−20.3
18	C_i–(C_B)(H)$_2$	+0.077	+40.5	−0.824	−20.2	+0.309	+42.6	−0.520	−17.0
19	C_i–(C_B)(C)(H)	−0.300	+42.3	−0.582	−28.2	−0.044	+44.6	−0.499	−27.6
20	C_i–$(C_B)(C)_2$	−1.294	+39.7	−0.693	−33.5	−0.976	+42.7	−0.581	−32.7
21	$C_{i,B}$	−0.031	−35.8	+0.084	+6.2	+0.354	−32.2	+0.144	+6.5
22	$C_{i,cyclo-5}$–(H)	−0.220	+11.9	−0.858	−25.3	−0.040	+13.5	−0.787	−24.8
23	$C_{i,cyclo-6}$–(H)	−0.462	+4.2	−0.028	−20.7	−0.262	+6.0	+0.060	−20.1
24	$C_{i,cyclo-6}$–(C)	−0.964	+1.6	−0.243	−30.8	−0.647	+4.5	−0.157	−30.2
25	$C_{i,cycloallylic-6}$–(C_d)(H)	−0.252	+54.0	−0.129	−37.5	+0.029	+56.5	−0.035	−36.8

range between −48.8 kJ mol^{-1} and 6.2 kJ mol^{-1}, again for resp. the C_2–$(C_d)_2$(C) and the $C_{2,B}$- group. For pre-exponential factors, the ΔGAV^{o}s range between −0.858 and 0.106, for resp. the $C_{2,cyclo\text{-}5}$–(H) and the $C_{2,d}$-(C_d) group. In general, the group additive values ΔGAV^{o} for activation energies of the cyclic reactants are similar to their linear equivalent within a few kJ mol^{-1}, but for the pre-exponential factor large differences are noticed, up to 0.87 for the difference between the $C_{2,cyclo\text{-}5}$-(H) and the C_2–$(C)_2$(H) group.

The ΔGAV^{o}s at other temperatures are given in Table S4 of the ESI. As illustrated in Fig. 7, the temperature dependence of the ΔGAV^{o}s is remarkably small: from 300 to 1000 K, the ΔGAV^{o}s for activation energies vary for 48 of the 50 ΔGAV^{o}s by less than 4 kJ mol^{-1}, and the ΔGAV^{o}s for pre-exponential factors log A by less than 0.4. For the $\Delta GAV^{o}(C_2)$, pertaining to groups describing the formed radical, the dependence is even smaller: for 24 of the 25 ΔGAV^{o}s the changes remain below 1 kJ mol^{-1} on $\Delta GAV^{o}_{E_a}$ and 0.1 on $\Delta GAV^{o}_{\log A}$. The larger deviations all pertain to reactions in which one of the reactants has a free rotor that is obviously not present in the reference reaction: the abstraction from toluene, in which the free methyl rotor of toluene is lost in the transition state (group C_2–$(C_b)(H)_2$), and the abstractions by the 3-methylpenta-1,4-dien-3-yl and 3-methylpenta-1,4-diyn-3-yl radicals, in which a free methyl rotor is lost in the transition state (groups C_1–$(C_d)_2$(C) and C_1–$(C_t)_2$(C)). The limited temperature dependence of the ΔGAV^{o} allows their use over a broad temperature range, in particular at higher temperatures, without much loss of accuracy. The accuracy also benefits by the compensation of the limited increase in ΔGAV^{o} for log A with increasing temperature with the increase in ΔGAV^{o} for E_a with temperature.

3.3.2 Resonance corrections. In this section, the contributions to E_a and log A arising from resonance and hyperconjugative effects in the transition state that cannot be included in the ΔGAV^{o} are discussed. As already mentioned, these contributions account for the additional resonance and hyperconjugative effects due to the simultaneous presence of groups centered on C_1 and on C_2. According to eqn (6) and

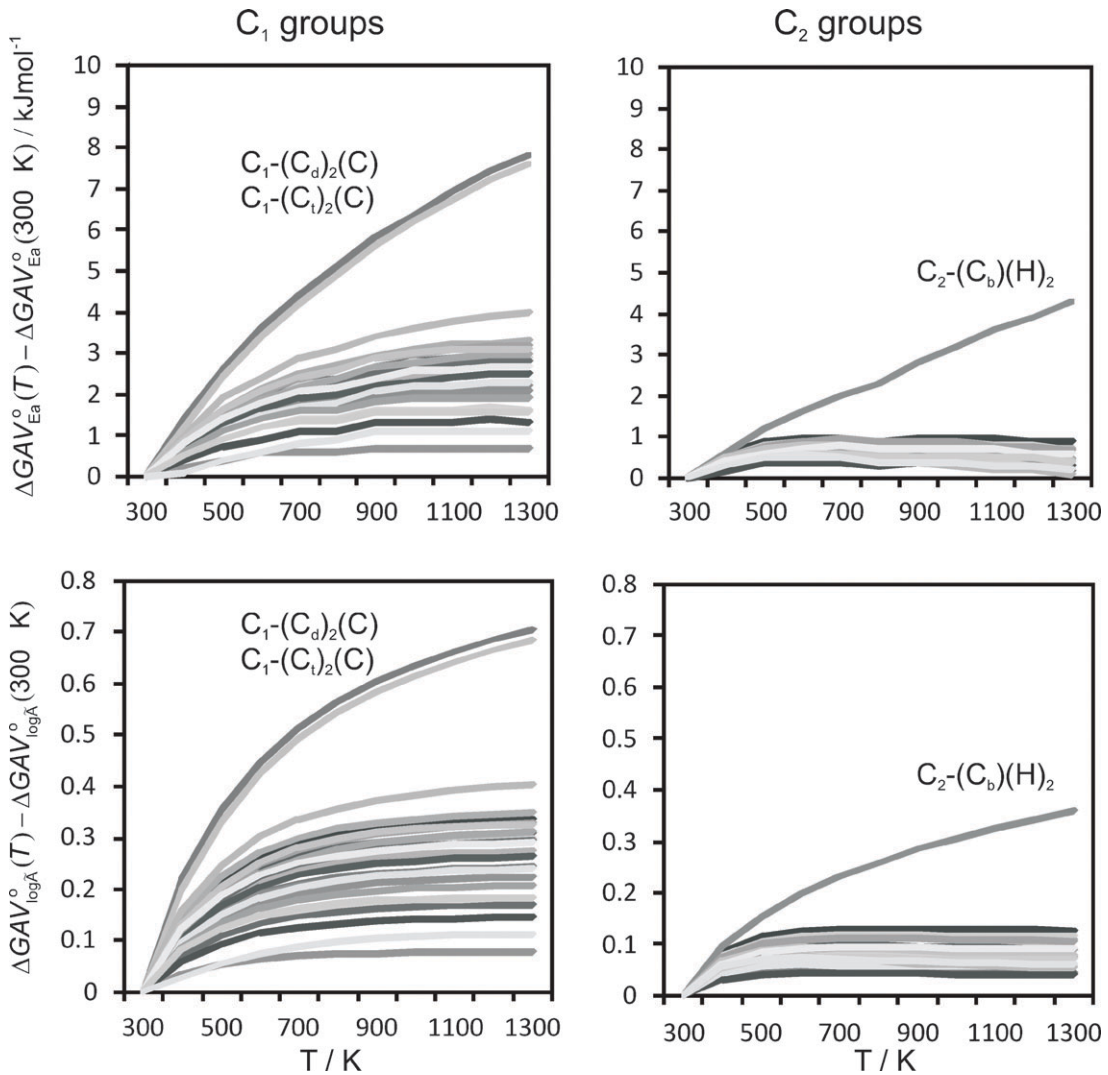

Fig. 7 Temperature dependence of the group additive values: difference of ΔGAV^{o}s with ΔGAV^{o}(300 K).

(8), the observed effects of resonance stabilization on the activation energy can be defined as

$$\Delta E^{\circ}_{\text{resonance}} = E_a(T) - \left(E_{a,\text{ref}}(T) + \sum_{i=1}^{2} \Delta GAV^{\circ}_{E_a}(C_i) \right) \quad (11)$$

and on the pre-exponential factor as

$$\Delta \log \tilde{A}_{\text{resonance}} = \log \tilde{A}(T) - \left(\log \tilde{A}_{\text{ref}}(T) + \sum_{i=1}^{2} \Delta GAV^{\circ}_{\log \tilde{A}}(C_i) \right) \quad (12)$$

The effect of resonance stabilization for the reactions of Table 2 is summarized in Table 5. Since the cross-resonance stabilization pertains to the transition state only, the observed resonance stabilization according to eqn (11) and (12) is independent of the direction of the reaction. The applied symmetry numbers in the group additive modeling can be found in Table S3 of the ESI, and the observed resonance stabilizations at 600 and 1000 K in Tables S5–S6.†

The reactions in Table 5 are grouped according to the types of cross-resonance and cross-hyperconjugation interactions proposed in section 3.2. First the resonance stabilization of the activation energy is discussed, followed by the pre-exponential factor.

The first type of resonance stabilization, *i.e.* the $\pi_{=}$–$\pi_{=}$ interaction, pertains to reactions between allylic structures, for which the resonance stabilization $\Delta E^{\circ}_{\text{resonance}}$ amounts up to −25 kJ mol^{-1} for the H abstraction between tertiary allylic structures (reaction 32, Table 5). The $\pi_{=}$–$\pi_{=}$ stabilization is closely followed by the. $\pi_{=}$–$\pi_{\equiv}$ stabilization occurring in the H transfer between allylic and propargylic radicals (reactions 33–35, Table 5). For these reactions, the resonance energy is only 1 to 3 kJ mol^{-1} smaller in magnitude than for the equivalent reactions between two allylic radicals, suggesting the use of a single correction to account for both types of resonance stabilization in order to reduce the number of parameters. For the third type of resonance stabilization, *i.e.* the $\pi_{\equiv}$–$\pi_{\equiv}$ interaction, pertaining to hydrogen transfer between two propargylic radicals, the resonance effects are 3 to 6 kJ mol^{-1} smaller than for the the $\pi_{=}$–$\pi_{=}$ interaction. Note that within these three categories, there is a clear trend of increasing stabilization with increasing number of methyl substituents on the radical center due to the stabilizing π–$\sigma_{\beta C-H}$ hyperconjugative interaction between the allylic π system and the methyl C–H bonds. Each additional methyl substituent on the radical center increases the stabilization energy by some −3 to −4 kJ mol^{-1}. This π–$\sigma_{\beta C-H}$ hyperconjugative effect is further evident from the reactions between resonance-stabilized and alkylic radicals (reactions 41–46, Table 5). For these reactions, the resonance stabilization amounts from −2 to −11 kJ mol^{-1}, depending on the number of methyl substituents on the radical center. The hyperconjugative $\sigma_{\beta C-H}$–$\sigma_{\beta C-H}$ interaction occurring in H transfer between alkylic radicals (reactions 47–48, Table 5) is rather small. Even for reactions between tertiary alkylic radicals, for which the maximum number of cross-hyperconjugation interactions is present in the transition state, the maximum stabilization amounts to −3.1 kJ mol^{-1}. Clearly, even for the reaction between these textbook examples of sterically hindered groups, a stabilizing interaction occurs, indicating the electronic nature of the stabilization and the absence of strong steric effects. The absence of steric effects is also evidenced by the very low barrier of 1.8 kJ mol^{-1} to internal rotation about the C–H–C bond for this reaction. However, the influences on the pre-exponential factor, which decrease up to a factor of 3 due to cross-hyperconjugation and are discussed further, are substantial enough to justify the inclusion of a correction for this interaction. With the current set of reactions only C–H hyperconjugation interactions were studied. The influence of C–C hyperconjugation is not considered, but based on bond dissociation enthalpies of various primary radicals the influence can be expected to be similar.[50]

To check the validity of the resonance model, also 6 reactions are included for which one of the reactants is not stabilized by resonance nor hyperconjugation (reactions 49–54, Table 5). For these reactions, no cross-conjugation effects in the transition state can be present. Indeed, no stabilization is observed for the reactions with these vinylic radicals; the formal value for $\Delta E^{\circ}_{\text{resonance}}$ ranges between −0.6 and 2.5 kJ mol^{-1}, indicating that even a small destabilization with respect to the reference reaction could be present. Note that the resonance-stabilized buta-1,3-dien-2-yl radical (reverse reaction 54, Table 5) adopts the butadiene structure prior to reaction, and therefore reacts as a non-resonance-stabilized vinylic radical (see Fig. S1 of the ESI).

The decreasing effect of cross-conjugation stabilization on the pre-exponential factor due to motional restriction imposed by the resonance, as discussed previously, is also shown by Table 5. For the first category, log A decreases between 0.2 and 0.8 depending on the number of substituents on the radical center. For the other categories, the influence is less pronounced although for the more substituted radicals the decrease can amount up to 0.5 on log A. This also pertains to the reactions in category 5, for which the hyperconjugative effect on the activation energy is limited but for which $\Delta \log A$ amounts up to 0.475, corresponding with an effect of a factor 3 on the pre-exponential factor.

The four corrections accounting for cross resonance/hyperconjugative interactions (see section 3.2) are determined by fitting to the values for $\Delta E^{\circ}_{\text{resonance}}$ and $\Delta \log \tilde{A}_{\text{resonance}}$ of Table 5 at 300, 600 and 1000 K (see Table 6). The applied number of corrections for the reactions in Table 5 are given in Table S7 of the ESI. The first type of cross-π-conjugation, the junction of the $\pi_{=}$–$\pi_{=}$ and $\pi_{=}$–$\pi_{\equiv}$ interactions denoted as $\pi_{=}$–$\pi_{=/\equiv}$ (correction 1), has the largest contribution to both the activation energy, −9.8 kJ mol^{-1}, and the pre-exponential factor, −0.180 on log A (300 K). The second type of cross-π-conjugation between propargylic radicals (correction 2, $\pi_{\equiv}$–$\pi_{\equiv}$) has a contribution of −6.2 kJ mol^{-1} to the activation energy, while its contribution to the pre-exponential factor is rather small and amounts to −0.067 only. For cross-π-hyperconjugative stabilization π–$\sigma_{\beta C-H}$ (correction 3), the correction on E_a is −3.4 kJ mol^{-1} per interaction, and −0.061 on log A. The values for the cross-hyperconjugative

Table 5 Resonance stabilization energies and effects of resonance on the pre-exponential factor, according to eqn (17) and (18), and remaining deviations between group additive prediction and *ab initio* value after correcting the group additive predictions with the resonance corrections of Table 6 (300 K)

		Resonance effect		Remaining deviations	
	Reaction	$\Delta E^{\circ}_{resonance}$/kJ mol^{-1}	$\Delta \log \tilde{A}_{resonance}$	$E_{a,pred}$–$E_{a,AI}$/kJ mol^{-1}	$\log A_{pred}$–$\log A_{AI}$
1.	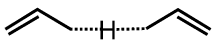				
27	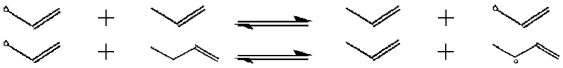	−10.4	−0.181	+0.6	+0.001
28	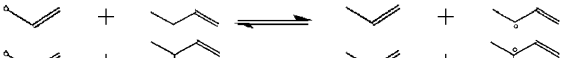	−13.4	−0.298	+0.2	+0.057
29	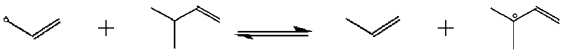	−18.0	−0.259	+1.4	−0.043
30	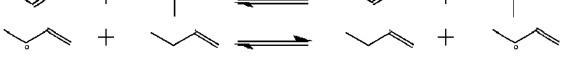	−18.9	−0.353	+2.0	+0.002
31	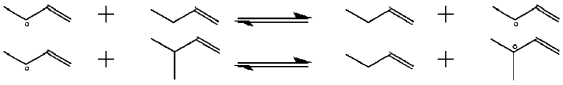	−20.7	−0.544	+0.1	+0.083
32		−24.5	−0.738	−0.1	+0.118
2.	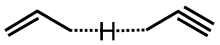				
33	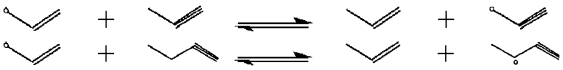	−8.3	−0.085	−1.5	−0.095
34	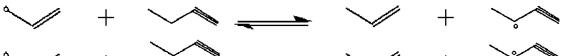	−11.9	−0.167	−1.3	−0.074
35	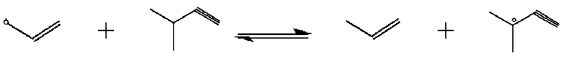	−15.0	−0.263	−1.6	−0.039
3.	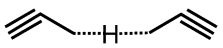				
36	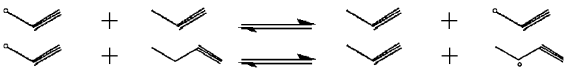	−5.6	−0.055	−0.6	−0.012
37	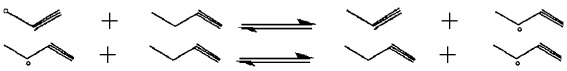	−9.5	−0.122	−0.1	−0.006
38		−13.4	−0.231	+0.1	−0.007
39	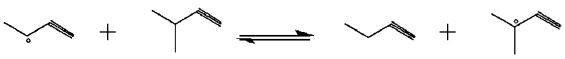	−17.4	−0.344	+0.4	−0.004
40	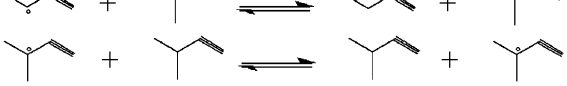	−20.9	−0.543	−0.1	+0.036
4.	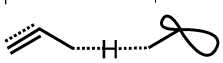				
41	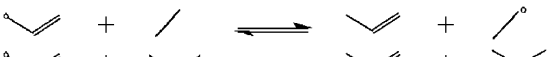	−3.6	−0.063	+0.2	+0.002
42	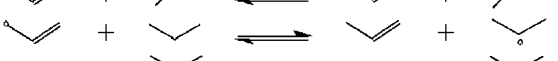	−7.6	−0.080	+0.8	−0.042
43		−9.5	−0.131	−0.7	−0.052
44	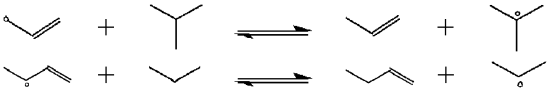	−6.8	−0.213	−0.6	−0.007
45	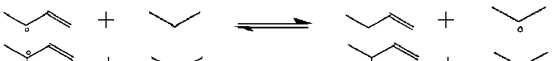	−7.8	−0.228	−0.2	−0.090
46	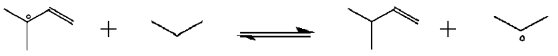	−10.9	−0.427	−1.1	−0.050
5.	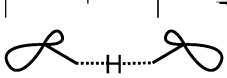				
47	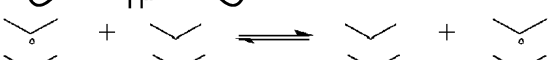	−0.8	−0.126	−0.4	−0.070
48	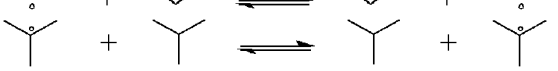	−3.1	−0.475	+0.4	+0.034
6. No resonance stabilization					
49	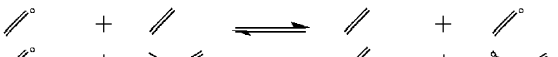	−0.6	−0.006	+0.6	+0.006
50	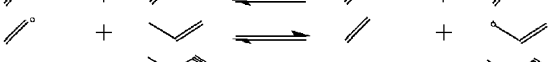	0.9	−0.048	−0.9	+0.048
51	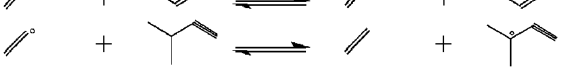	2.5	−0.079	−2.5	+0.079
52		−0.1	0.033	+0.1	−0.033
53	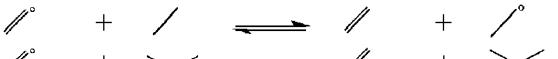	0.1	0.048	−0.1	−0.048
54	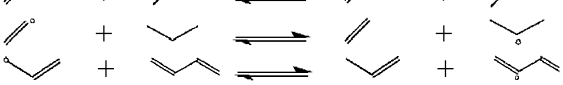	−0.1	0.033	+0.1	−0.033
		MD		−0.2	−0.009
		MAD		0.7	0.042

Table 6 Corrections for resonance stabilization of the transition state, with indication of the 97.5% confidence intervals (E_a in kJ mol^{-1})

			300 K		600 K		1000 K		Average	
	Correction	Corresponding structure	E_a	log A	E_a	log A	E_a	log A	E_a	log A
1	$\pi_{=}$–$\pi_{=/\equiv}$	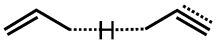	−9.8 ± 0.8	−0.180 ± 0.05	−10.0	−0.202	−10.1	−0.212	−9.9	−0.198
2	$\pi_{\equiv}$–$\pi_{\equiv}$	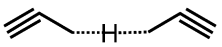	−6.2 ± 1.1	−0.067 ± 0.06	−5.7	−0.003	−5.5	0.008	−5.8	−0.021
3	π–$\sigma_{\beta C-H}$	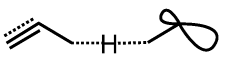	−3.4 ± 0.3	−0.061 ± 0.02	−3.3	−0.052	−3.4	−0.053	−3.4	−0.056
4	$\sigma_{\beta C-H}$–$\sigma_{\beta C-H}$	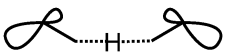	−0.3 ± 0.2	−0.049 ± 0.01	−0.3	−0.050	−0.3	−0.051	−0.3	−0.050

stabilization $\sigma_{\beta C-H}$–$\sigma_{\beta C-H}$ correction (correction 4) are very small, −0.3 kJ mol^{-1} on E_a and −0.049 on log A per interaction; both corrections are however significantly different from zero (see Table 6). Since the number of type 4 interactions add up easily, *e.g.*, 6 corrections for the reaction between a tertiary alkylic radical and a secondary group, the influence on the Arrhenius parameters can be considerable. The corrections for the activation energy are slightly temperature dependent: from 300 to 1000 K the largest change pertains to 0.7 kJ mol^{-1} for the $\pi_{\equiv}$–$\pi_{\equiv}$ correction. This same correction also exhibits the largest temperature dependence for the Δ log $\tilde{A}_{resonance}$ terms and this correction is only at 300 K significantly different from zero (determined for 97.5% confidence intervals). All other corrections are significant in the range of 300–1000 K. The limited temperature dependence allows, similar to ΔGAV^{o}, the use over a broad temperature range without losing much accuracy.

As illustrated in Table 5, the proposed method accurately describes the resonance stabilization. In combination with the group additive model, the MAD between the predicted and *ab initio* activation energies in Table 5 amounts to only 0.7 kJ mol^{-1}, compared to 9.4 kJ mol^{-1} without the cross-resonance corrections. For pre-exponential factors, the introduction of cross-resonance corrections reduces the MAD between the GA prediction and *ab initio* log A reduces from 0.219 to 0.042 (see Table 5). The deviations for category 6 remain unchanged, since no resonance corrections pertain to these reactions.

To illustrate the applicability of the proposed correction method, the total resonance/hyperconjugative correction is calculated for the abstraction of the allylic hydrogen atom from 1-butyne by 3-methyl-1-butyn-3-yl (see Fig. 8) at 300 K. The number of cross resonance and hyperconjugative interactions between the structures on C_1 and those on C_2 can be determined as follows. A single $\pi_{\equiv}$–$\pi_{\equiv}$ correction (type 2) is needed to account for the cross-π-conjugation between the two propargylic structures. Next, three cross-π-hyperconjugative interactions π–$\sigma_{\beta C-H}$ (type 3) can be identified: two π–$\sigma_{\beta C-H}$ interactions between the propargyl fragment on C_1 and the 2 methyl substituents on C_2, and one π–$\sigma_{\beta C-H}$ interaction interaction between propargyl fragment on C_2 and the methyl substituent on C_1. Finally, 2 $\sigma_{\beta C-H}$–$\sigma_{\beta C-H}$ corrections account for the cross-hyperconjugation between the methyl substituent on C_1 and the 2 methyl substituents an C_2. This yields following value for the resonance energy:

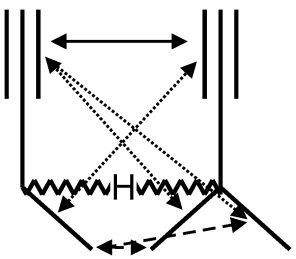

Fig. 8 Resonance interactions in the transition state of the H-abstraction from the propargylic H of 1-butyne by 3-me-1-butyn-3-yl. The plot shows the $\pi_{\equiv}$–$\pi_{\equiv}$ correction (full line), the π–$\sigma_{\beta C-H}$ corrections (dotted line) and the $\sigma_{\beta C-H}$–$\sigma_{\beta C-H}$ corrections (dashed line).

$$\Delta E^{o}_{resonance} = 1\ \pi_{\equiv}\text{–}\pi_{\equiv} + 3\ \pi\text{–}\sigma_{\beta C-H} + 2\ \sigma_{\beta C-H}\text{–}\sigma_{\beta C-H}$$
$$= 1(-6.2) + 3(-3.4) + 2(-0.3) = -17.0 \text{ kJ mol}^{-1}$$

agreeing well with the observed stabilization energy of −17.4 kJ mol^{-1} (reaction 39). In order to obtain the activation energy, this resonance energy should be added to the group additively predicted activation energy. The effect on the pre-exponential factor is:

$$\Delta\log A_{resonance} = 1\ \pi_{\equiv}\text{–}\pi_{\equiv} + 3\ \pi\text{–}\sigma_{\beta C-H} + 2\ \sigma_{\beta C-H}\text{–}\sigma_{\beta C-H}$$
$$= 1(-0.067) + 3(-0.061) + 2(-0.049)$$
$$= -0.348$$

which is only 0.004 off the observed resonance effect on log A of −0.344.

3.4 Tunneling model

As discussed in section 2.3, the reported group additive values do not include tunneling contributions. The contribution of tunneling to the rate coefficients, which is mainly dependent on the electronic barrier to tunneling and the imaginary frequency in the transition state, cannot be predicted directly by group additivity. Therefore, in this section, the tunneling is correlated with the Arrhenius activation energy, which is a good measure for the electronic tunneling barrier and can be predicted using group additivity. The activation energy considered pertains to the smallest value among the forward- and reverse activation energy, *i.e.* the activation energy of the exothermic reaction

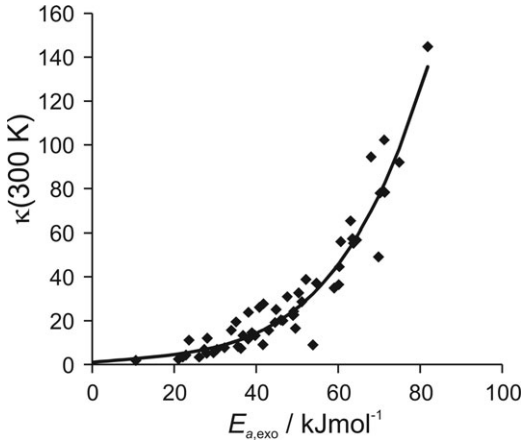

Fig. 9 Tunneling coefficients as function of the *ab initio* activation energy, for the reactions from Tables 1 and 2 (dots) and the fit from eqn (10) (the reaction $CH_3^o + H_2$ is excluded).

$E_{a,exo}$, as tunneling can only proceed through the net electronic barrier that excludes contributions from reaction endothermicity. Therefore, prior to the calculation of the tunneling correction the activation energy for both the forward and the reverse reaction needs to be calculated using the ΔGAV^o and resonance corrections presented above.

Fig. 9 presents the Eckart tunneling coefficients for the reactions in Tables 1 and 2*versus* the *ab initio* activation energy $E_{a,exo}$ at 300 K. The actual Eckart tunneling coefficients for all reactions are shown in Table S8 of the ESI (300–1000 K). A fourth order polynomial with temperature-dependent coefficients allowed to fit the data. The second and third order terms were not significant. The following polynomial:

$$\kappa(T) = 1 + \left(\frac{162}{T}\right)^3 (E_{a,exo}) + 2.71 \times 10^{-6} \exp\left(-\frac{T-300}{26}\right)(E_{a,exo})^4 \quad (13)$$

could describe the 54 tunneling coefficients in the range 300–1000 K with a mean factor of deviation $\langle\rho\rangle$ of only 1.15. The only deviation larger than 2 is for the reaction 1,3-butadien-2-yl + propene at 300 and 400 K (reaction 54).

4. Application and validation of the model

In this section, the group additivity is validated by comparison of the rate coefficients calculated by group additivity with those obtained from *ab initio* calculations and with experimental rate coefficients.

We first demonstrate the application of the group additive method by calculating two examples, starting with the rate coefficient for the abstraction of the allylic hydrogen of propene by the penta-1,4-dien-3-yl (1000 K).

The groups related to this reaction are the C_1–$(C_d)_2(H)$ group for the abstracting radical and the C_2–$(C_d)(H)_2$ group for the group from which the hydrogen is abstracted. The resonance corrections involved in this reaction are 2 $\pi_{=}$–$\pi_{=/\equiv}$ cross-π-conjugation corrections, since there are 2 allylic fragments on C_1 and 1 allylic fragment on C_2. The activation energy can thus be obtained as:

$$\begin{aligned} E_a(1000\text{ K}) &= E_{a,ref}(1000\text{ K}) + \Delta GAV^o_{E_a}[C_1 - (C_d)_2(H)] \\ &\quad + \Delta GAV^o_{E_a}[C_2 - (C_d)(H)_2] + 2\pi_{=} - \pi_{=/\equiv} \\ &= 84.4 + 89.5 - 26.5 + 2(-10.1) = 127.2\text{ kJ mol}^{-1} \end{aligned}$$

which differs only by 1.3 kJ mol^{-1} from the *ab initio* calculated value of 125.9 kJ mol^{-1}. The pre-exponential factor can be determined as

$$\begin{aligned} \log A(1000\text{ K/m}^3\text{ mol}^{-1}\text{ s}^{-1}) &= \log \tilde{A}_{ref}(1000\text{ K}) \\ &+ \Delta GAV^o_{\log\tilde{A}}[C_1\text{–}(C_d)_2(H)] + \Delta GAV^o_{\log\tilde{A}}[C_2\text{–}(C_d)(H)_2] \\ &+ 2\,\pi_{=}\text{–}\pi_{=/\equiv} + \log n_e = 6.509 + 0.658 - 0.535 \\ &+ 2(-0.212) + \log 12 = 7.287 \end{aligned}$$

which is again in perfect agreement with the *ab initio* determined value for $\log(A/\text{m}^3\text{ mol}^{-1}\text{ s}^{-1})$ of 7.291. The tunneling coefficient for this reaction is determined using expression (13). The smallest activation energy for this reaction is the activation energy of the exothermic reverse reaction, which amounts to 72.6 kJ mol^{-1} = 84.4 − 42.9 + 51.3 + 2(−10.1). The tunneling coefficient resulting from expression (13) is, at 1000 K using a barrier of 72.6 kJ mol^{-1}, 1.31. With this information the rate coefficient can be calculated:

$$\begin{aligned} k(1000\text{ K}) &= 1.31 \times 10^{7.287} \exp\left(-\frac{127.2\text{ kJ mol}^{-1}}{RT}\right) \\ &= 5.8\text{ m}^3\text{ mol}^{-1}\text{ s}^{-1} \end{aligned}$$

The *ab initio* rate coefficient is 6.7 m^3 mol^{-1} s^{-1}, which agrees well with the group additively determined rate coefficient.

As a second example, the rate coefficient for the abstraction by an ethyl radical from the propargylic hydrogen of 1-butyne (300 K) is calculated:

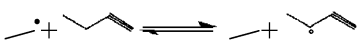

The kinetics for this reaction are described using the C_1–$(C)(H)_2$ group for the abstracting radical and the C_2–$(C_t)(C)(H)$ group for the formed radical. In the transition state, two types of cross-hyperconjugative corrections can be distinguished. The first one pertains to π–$\sigma_{\beta C-H}$, describing the interaction between the methyl substituent of the abstracting radical and the triple bond adjacent to the abstracted hydrogen. The second one pertains to $\sigma_{\beta C-H}$–$\sigma_{\beta C-H}$ for the interaction between the two methyl substituent. Using these contributions, the activation energy is obtained as:

$$\begin{aligned} E_a(300\text{ K}) &= E_{a,ref}(300\text{ K}) + \Delta GAV^o_{E_a}[C_1 - (C)(H)_2] \\ &\quad + \Delta GAV^o_{E_a}[C_2 - (C_t)(C)(H)] + \pi - \sigma_{\beta C-H} \\ &\quad + \sigma_{\beta C-H} - \sigma_{\beta C-H} \\ &= 69.7 + 4.7 \\ &\quad - 31.8 + (-3.4) + (-0.3) \\ &= 38.9\text{ kJ mol}^{-1} \end{aligned}$$

which differs only by 0.1 kJ mol^{-1} from the *ab initio* calculated value of 38.8 kJ mol^{-1}. The pre-exponential factor is determined as

$$\log A(300\ \mathrm{K/m^3\ mol^{-1}\ s^{-1}}) = \log \tilde{A}_{\mathrm{ref}}\,(300\ \mathrm{K}) + \Delta GAV^{\circ}_{\log \tilde{A}}[\mathrm{C_1}\text{–}(\mathrm{C})(\mathrm{H})_2] + \Delta GAV^{\circ}_{\log \tilde{A}}[\mathrm{C_2}\text{–}(\mathrm{C_t})(\mathrm{C})(\mathrm{H})] + + \pi\text{–}\sigma_{\beta \mathrm{C-H}} + \sigma_{\beta \mathrm{C-H}}\text{–}\sigma_{\beta \mathrm{C-H}} + \log n_e = 5.267 - 0.866 - 0.044 - 0.061 - 0.049 + \log 4 = 4.850$$

differing only 0.07 with the *ab initio* determined value for $\log(A/\mathrm{m^3\ mol^{-1}\ s^{-1}})$ of 4.923. With 38.9 kJ mol^{-1} as the smallest activation energy among the forward and reverse activation energy, the tunneling coefficient calculated using expression (13) is, at 300 K, 13.3. This yields for the rate coefficient:

$$k(300\ \mathrm{K}) = 13.3 \times 10^{4.850} \exp\left(-\frac{38.9\ \mathrm{kJ\ mol^{-1}}}{RT}\right) = 0.16\ \mathrm{m^3\ mol^{-1}\ s^{-1}}$$

which is within 50% of the *ab initio* rate coefficient of 0.26 m^3 mol^{-1} s^{-1}. The major part of the deviation can be traced back to the tunneling coefficient, which amounts to 18.5 in the Eckart approximation.

4.1 *Ab initio* validation

To validate the group additivity method, group additive predictions are compared to *ab initio* obtained values for a set of 19 reactions that have not been used previously to determine group additive values or resonance corrections. These reactions have been chosen to represent a variety of reactants and resonance stabilization. Table 7 and 8 illustrate that for hydrogen transfer reactions that involve reactants included in the reactions to determine the ΔGAV°s (see Table 1), the deviations between the group additive predicted and *ab initio* values are identical for the forward and reverse reaction; for these reactions, the deviation pertains only to differences between the group additively predicted and actual transition state. This is no longer the case when one of the reactants differs from those of Table 1, as for these reactions not only the transition state but also the reactants differ. Therefore in Tables 7 and 8, deviations for both forward and reverse reactions are included. The calculation of the number of single events and the applied number of resonance corrections can be retrieved in Tables S9–S10 of the ESI.

First, pre-exponential factors, activation energies and tunneling coefficients are compared at 300 and 1000 K, see Table 7. The applied group additive values and resonance corrections are 300 and 1000 K values resp., as reported in Table 3 and Table 6. The actual *ab initio* and group additive kinetic parameters are given in Tables S11–S12 of the ESI. At 300 K, the pre-exponential factors are predicted with a maximum deviation of a factor of 7. The largest discrepancy is noticed for the hydrogen abstraction between a methyl radical and 2,3-dimethylbut-2-ene (reaction 10), for which the pre-exponential factor is overestimated by a factor of 7. This is an exception however: 75% of the pre-exponential factors are correctly reproduced within a factor of 2 with respect to the *ab initio* obtained value.

For the activation energies, the predictions are within 6 kJ mol^{-1} of the *ab initio* values; the largest deviation is observed for the reaction of a neopentyl radical with methane (reaction 9). For 75% of the reactions, activation energies are predicted within 3 kJ mol^{-1}. Tunneling coefficients are also reproduced in an excellent way. At 1000 K, the deviations between prediction and *ab initio* calculation are of the same magnitude, only the tunneling is obviously better predicted since the tunneling coefficients are much smaller.

The comparison of the predicted rate coefficients with *ab initio* rate values is given in Table 8, again at 300 and 1000 K. The overall agreement can be considered as excellent. At 300 K, the overall mean factor of deviation $\langle \rho \rangle$ amounts to 2.4. Ratios range between 0.18 and 5.8. For 4 of the 19 reactions, the factors of deviation ρ are larger than 4. Comparison with *ab initio* rate coefficients at 1000 K yields, on the same set of reactions, an overall mean factor of difference of 1.8. All but 2 rate coefficients are predicted within a factor of 4, while for 11 of the 19 reaction the rate coefficients are predicted within a factor of 2.

As thermodynamic consistency is of importance for many applications, the reaction equilibria obtained from group additive rate predictions are compared to the *ab initio* calculated equilibrium using the ratio $K^{\mathrm{eq}}_{\mathrm{GA}}/K^{\mathrm{eq}}_{\mathrm{AI}}$ in Table 8. As mentioned above, for reactions involving reactants of Table 1 that have been used to determine the ΔGAV°s, the predicted equilibrium coefficients are identical to the *ab initio* equilibrium coefficients. At 300 K, the deviations from the *ab initio* equilibrium coefficients can amount up to a factor 10, which reduces to a maximal factor of 4.5 at 1000 K. The largest deviations are observed for the reaction with *cis*-2-butene (reaction 3) and reactions with isobutyl radicals (reactions 8 and 15). Accounting for secondary and tertiary contributions, which are neglected in the truncated group additivity method, might reduce the deviations to an acceptable level for use in reaction networks. However, as inclusion of these contributions is already difficult for thermochemistry it can be expected that it will be even more difficult in the modeling of kinetics.[21] Therefore, it is recommended to implement thermodynamic consistency explicitly by calculating the reverse rate coefficient from the forward rate and the thermodynamic equilibrium coefficient. The thermodynamic equilibrium can be calculated using thermochemical group additivity, which predicts equilibrium coefficients more reliably, typically within a factor of 2.[51]

4.2 Experimental validation

In Table 9, the group additive predictions are compared with experimental values from literature. The experimental rate coefficients are taken from the NIST Chemical Kinetics web site[52] for all hydrogen abstractions between hydrocarbons for which experimental data was available, excluding the data that have already been used in the level of theory study reported by Vandeputte *et al.*[31] Also, rate coefficients from the compilations of Tsang for which Tsang indicated the rate coefficients to be predictions were excluded.[53] From the resulting set of 17 hydrogen abstractions, 10 rate coefficients are determined by fitting to complex reaction mechanisms. As

Table 7 Group additive validation: comparison of the group additive pre-exponential factor and activation with *ab initio* values, and comparison of the predicted tunneling coefficient κ with the Eckart value (f: forward, r: reverse)

		300 K			1000 K		
	Reaction	κ/κ_{AI}	$\frac{A_{GA}}{A_{AI}}$	$E_{a,GA}-E_{a,AI}$	κ/κ_{AI}	$\frac{A_{GA}}{A_{AI}}$	$E_{a,GA}-E_{a,AI}$
1f	$CH_3^\circ + \rightleftharpoons CH_4 +$	1.03	0.94	−0.9	0.99	0.95	−0.8
1r			1.21	+2.1		1.10	+1.8
2f	$CH_3^\circ + \rightleftharpoons CH_4 +$	1.14	3.89	+0.8	0.99	3.90	+0.7
2r			1.11	+1.9		1.09	+1.8
3f	$CH_3^\circ + \rightleftharpoons CH_4 +$	1.37	1.69	+5.7	1.02	1.67	+5.8
3r			3.26	+1.6		3.04	+1.3
4f	$CH_3^\circ + \rightleftharpoons CH_4 +$	1.21	1.03	+0.6	1.07	1.05	+0.7
4r			1.40	−1.1		1.32	−1.4
5f	$CH_3^\circ + \rightleftharpoons CH_4 +$	1.11	1.10	+0.5	1.01	1.11	+0.5
5r			2.00	+5.7		1.14	+2.9
6f	$CH_3^\circ + \rightleftharpoons CH_4 +$	1.16	3.05	+0.2	0.97	3.05	+0.2
6r			1.00	+1.2		0.99	+1.2
7f	$CH_3^\circ + \rightleftharpoons CH_4 +$	1.05	1.25	+0.8	1.04	1.26	+0.8
7r			1.35	+1.8		1.33	+1.8
8f	$CH_3^\circ + \rightleftharpoons CH_4 +$	1.13	3.69	+0.7	0.99	3.67	+0.6
8r			1.14	+3.2		1.09	+3.0
9f	$CH_3^\circ + \rightleftharpoons CH_4 +$	1.05	1.06	+1.6	1.01	0.91	+0.9
9r			1.82	+6.0		1.77	+5.9
10f	$CH_3^\circ + \rightleftharpoons CH_4 +$	1.33	7.42	+4.8	1.08	7.41	+4.9
10r			0.83	−2.7		0.69	−3.5
11f	$CH_3^\circ + \rightleftharpoons CH_4 +$	1.07	4.65	+2.3	0.96	4.51	+2.2
11r			4.15	+4.1		4.12	+4.0
12f	$+ \rightleftharpoons +$	0.85	0.87	−0.4	0.99	0.88	−0.3
12r			0.87	−0.5		0.89	−0.3
13f	$+ \rightleftharpoons +$	0.72	0.85	+0.1	0.97	0.83	+0.1
13r			0.84	+0.1		0.83	+0.1
14f	$+ \rightleftharpoons +$	0.75	0.46	+0.2	0.90	0.46	+0.2
14r			0.46	+0.2		0.46	+0.2
15f	$+ \rightleftharpoons +$	0.84	5.55	−0.6	0.99	5.84	−0.4
15r			1.71	+1.9		1.73	+2.0
16f	$+ \rightleftharpoons +$	0.81	1.04	+1.6	1.00	0.99	+1.4
16r			1.04	+1.6		0.99	+1.4
17f	$+ \rightleftharpoons +$	0.63	0.64	−2.4	0.94	0.76	−2.0
17r			0.64	−2.4		0.76	−2.1
18f	$+ \rightleftharpoons +$	0.63	0.86	−3.8	1.12	1.09	−3.2
18r			0.86	−3.7		1.09	−3.2
19f	$+ \rightleftharpoons +$	0.78	1.45	+3.6	0.95	1.36	+3.4
19r			1.29	+3.4		1.05	+2.8
	mean $\langle\rho\rangle$ value/MAD	1.23	2.00	+2.0	1.04	1.95	+1.8

the rate coefficients for these reactions might be biased by an incomplete reaction network, they are reported separately in Table 9. The rate coefficients are compared at 600 K for the reactions for which this temperature is in the experimental

Table 8 *Ab initio* rate coefficients, ratios between the group additive prediction and *ab initio* rate coefficient and equilibrium coefficient ($m^3\ mol^{-1}\ s^{-1}$)

		300 K			1000 K		
	Reaction	k_{AI}	$\frac{k_{GA,\kappa}}{k_{AI}}$	$\frac{K_{GA}^{eq}}{K_{AI}^{eq}}$	k_{AI}	$\frac{k_{GA,\kappa}}{k_{AI}}$	$\frac{K_{GA}^{eq}}{K_{AI}^{eq}}$
1f	CH_3° +  ⇌ CH_4 + 	5.7E-06	1.45	2.6	4.1E+02	1.05	1.2
1r		1.8E-01	0.57		1.5E+04	0.91	
2f	CH_3° +  ⇌ CH_4 + 	1.6E-03	3.40	5.5	2.2E+03	3.65	4.1
2r		1.5E-06	0.62		1.2E+02	0.90	
3f	CH_3° +  ⇌ CH_4 + 	2.8E+00	0.24	0.1	3.1E+04	0.86	0.3
3r		2.6E-14	2.47		2.1E+00	2.66	
4f	CH_3° +  ⇌ CH_4 + 	6.5E-01	1.02	0.4	2.7E+04	0.99	0.6
4r		2.2E-14	2.87		3.5E+00	1.61	
5f	CH_3° +  ⇌ CH_4 + 	6.4E-01	1.04	4.3	2.5E+04	1.06	1.3
5r		5.2E-13	0.24		1.4E+01	0.82	
6f	CH_3° +  ⇌ CH_4 + 	1.6E-03	3.41	4.6	2.7E+03	3.06	3.5
6r		1.3E-06	0.74		1.3E+02	0.88	
7f	CH_3° +  ⇌ CH_4 + 	1.1E-01	1.01	1.4	1.5E+04	1.16	1.1
7r		3.9E-07	0.72		9.3E+01	1.09	
8f	CH_3° +  ⇌ CH_4 + 	2.5E-03	3.34	9.0	3.5E+03	3.48	4.5
8r		2.6E-06	0.37		1.4E+02	0.77	
9f	CH_3° +  ⇌ CH_4 + 	1.8E-02	0.63	3.6	2.0E+04	0.83	0.9
9r		5.4E-06	0.18		1.3E+02	0.88	
10f	CH_3° +  ⇌ CH_4 + 	9.0E-01	1.48	0.4	1.2E+04	4.26	3.9
10r		1.8E-14	3.49		5.2E+00	1.08	
11f	CH_3° +  ⇌ CH_4 + 	1.3E-03	2.06	2.3	1.2E+03	3.52	1.4
11r		1.1E-06	0.90		4.4E+01	2.57	
12f	 +  ⇌  + 	1.5E-03	0.92	1.0	7.1E+02	0.92	1.0
12r		2.3E-05	0.92		3.0E+02	0.91	
13f	 +  ⇌  + 	2.6E-01	0.60	1.0	3.8E+03	0.81	1.0
13r		3.6E-10	0.60		3.3E+01	0.81	
14f	 +  ⇌  + 	5.5E+00	0.34	1.0	2.2E+04	0.44	1.0
14r		2.7E-12	0.34		2.5E+01	0.44	
15f	 +  ⇌  + 	1.4E-11	5.84	9.1	2.3E+01	6.07	4.5
15r		3.9E-02	0.64		1.1E+03	1.36	
16f	 +  ⇌ +	1.0E-02	0.47	1.0	5.3E+03	0.84	1.0
16r		3.1E-12	0.46		6.7E+00	0.84	
17f	+ ⇌ +	3.5E+02	1.14	1.0	2.4E+04	0.92	1.0
17r		1.3E-09	1.13		4.5E+01	0.92	
18f	+ ⇌ +	2.7E+02	2.58	1.0	1.8E+04	1.53	1.0
18r		1.5E-13	2.60		5.1E+00	1.51	
19f	+ ⇌ +	9.7E-06	0.29	1.0	2.2E+02	0.86	1.2
19r		8.2E+01	0.27		9.6E+04	0.72	
	Overall $\langle\rho\rangle$		2.4			1.8	

temperature range. For experimental temperature ranges not containing 600 K the rate coefficients were evaluated at the center of the reported temperature range, using the 600 K ΔGAV°. The experimental rate coefficients and sources can be

Table 9 Experimental validation set. Source of the experimental data can be retrieved in Table S13 of the ESI

	Reaction	T/K	k_{exp}/m^3 mol^{-1} s^{-1}	Ref.	k_{calc}/k_{exp}	ρ
	Other					
1	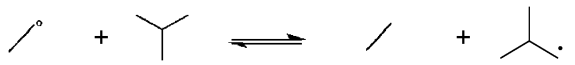	600	7.0×10^{-1}	53	0.54	1.9
2	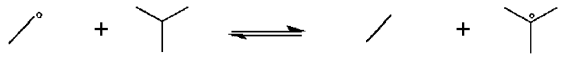	600	1.3×10^{0}	53	1.49	1.5
3	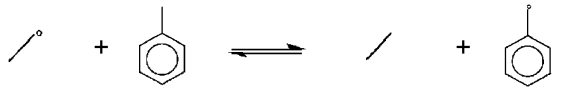	600	3.8×10^{1}	54	0.25	4.0
4		719	1.4×10^{0}	55	2.04	2.0
5		600	1.1×10^{-1}	53	2.12	2.1
6		600	1.0×10^{-2}	53	3.16	3.2
					$\langle\rho\rangle$	**2.5**
	Rate coefficients derived from complex reaction mechanisms					
7	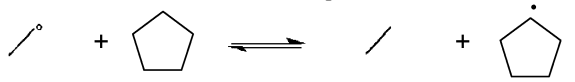	700	1.6×10^{2}	56	0.26	3.9
8	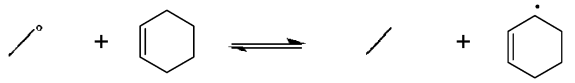	400	1.7×10^{3}	57	0.01	97.4
9	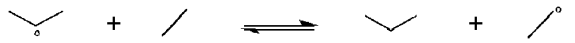	500	2.3×10^{-1}	58	0.76	1.3
10	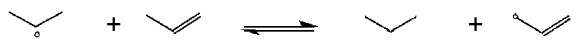	522	3.1×10^{0}	58	3.72	3.7
11	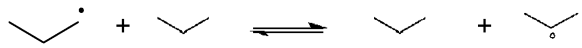	350	1.2×10^{-2}	59	0.60	1.7
12	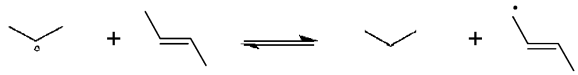	490	2.8×10^{0}	60	4.46	4.5
13		542	1.5×10^{-1}	61	7.07	7.1
14		515	1.0×10^{1}	62	4.06	4.1
15		817	1.1×10^{2}	63	0.04	26.7
16	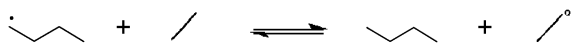	911	1.3×10^{2}	64	1.71	1.7
17	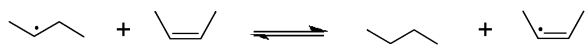	784	1.5×10^{3}	65	0.01	111.5
					$\langle\rho\rangle$	**24.0**

retrieved in Table S13 of the ESI. The calculation of the number of single events for the reactions and the applied groups and number of resonance corrections can be found in Table S14 of the ESI.

For the first set of reactions in Table 9, the mean factor of deviation $\langle\rho\rangle$ amounts to 2.5 while it amounts to 24 for the set of rate coefficients derived by fitting. The latter deviation is caused mainly by reaction 8 and 17, for which a ρ value of, respectively 97 and 111 is observed. As the group additively determined values for these reactions agree well with the *ab initio* based values (see reactions 14 and 19 in Table 8), this large deviations from the experimental value are not due to limitations in the group additive method. Next to these reactions, there are three more reactions for which the ρ value exceeds a factor of 4. In view of the excellent performance of the group additive method in comparison with *ab initio* calculated rate coefficients, *vide supra*, and the good agreement between CBS-QB3 and experimental rate coefficients of a mean factor of deviation of 3.9 at 600 K,[31] the experimental rate coefficients of reactions 8, 13, 15 and 17 can be regarded questionable with respect to influence of incomplete reaction networks on the fitted rate coefficients. Similar reactions in the set of Table 8 did not reveal problems related to the group additive modeling or to modeling of tunneling contributions. Therefore, ignoring the experimental rate coefficients derived by fitting to complex mechanisms, it can be concluded that, at 600 K, the methodology presented in this work allows obtaining rate coefficients for hydrogen abstraction reactions with a mean factor of deviation $\langle\rho\rangle$ of 2.5 between group additive predictions and experimental rate coefficients.

5. Conclusions

This study presents a consistent group additive model to predict the rate coefficients of hydrogen abstraction reactions between hydrocarbons in the range 300–1300 K, based on the model of Saeys *et al*.[20] The model is developed based on high-accuracy *ab initio* kinetics, using the CBS-QB3 method with corrections for internal rotation about the forming/breaking bond in the transition state and Eckart tunneling corrections, an approach which has previously shown its accuracy in comparison with experimental rate coefficients for these reactions.[31]

Cross-resonance and cross-hyperconjugation stabilization of the transition state is shown to have a significant influence on the energy and internal flexibility of the transition state. The derived group additive models account for a wide range of possible reactants for hydrogen abstractions. As expected from the construction of the method, the temperature dependence of these ΔGAV^{o} is very low, which allows the use of a set ΔGAV^{o} over a broad temperature range without loss of accuracy. For reactions between hyperconjugative and resonance-stabilized radicals, cross-conjugation and cross-hyperconjugation effects in the transition state can be well described using 4 corrections based on the topology of the transition state. The tunneling coefficients, which are strongly dependent on the barrier height, can be predicted using a polynomial of fourth order in the group additive activation energy of the exothermic direction of the reaction.

The resulting model performs very well in predicting 19 *ab initio* calculated rate coefficients: the mean factor of deviation $\langle\rho\rangle$ between the group additive prediction and the *ab initio* calculated rate coefficients for 19 reactions amounts to 2.4 at 300 K and 1.8 at 1000 K. The predictions also compare well to experimental rate coefficients, with a mean factor of deviation of 2.5. Hence, the proposed model, which can describe a wide variety of gas-phase hydrogen abstractions between hydrocarbons in the range 300–1300 K, can be considered to provide reliable rate coefficient predictions.

Notation

A	Pre-exponential factor $m^3\ mol^{-1}\ s^{-1}$
$\tilde{A}$	Single-event pre-exponential factor $m^3\ mol^{-1}\ s^{-1}$
$\Delta E(0\ K)$	Activation barrier at 0 K (including ZPVE) J mol^{-1}
$\Delta E^{o}_{E_a,res}$	cross-conjugation contribution to the activation energy J mol^{-1}
ΔGAV^{o}	Group Additive Value of kinetic parameter, referred to the value of the reference reaction $m^3\ mol^{-1}\ s^{-1}$ or J mol^{-1}
$\Delta \log \tilde{A}_{resonance}$	cross-conjugation contribution to the pre-exponential factor
E_a	Activation energy J mol^{-1}
$E_{a,exo}$	activation energy of the exothermic direction of the reaction J mol^{-1}
k_∞	high pressure rate coefficient $m^3\ mol^{-1}\ s^{-1}$ or s^{-1}
$\kappa(T)$	tunneling coefficient —
n_e	Number of single events —
n_{opt}	Number of optical isomers —
p	Pressure Pa
q	Molecular partition function —
ρ	factor of deviation —
T	Temperature K
σ	Symmetry number (ext: external, int: internal) —

Acknowledgements

M.K.S. held a PhD grant of the Institute for the Promotion of Innovation through Science and Technology in Flanders (IWT-Vlaanderen) and is grateful for financial support from the Fund for Scientific Research-Flanders (F.W.O.-Vlaanderen). Aäron G. Vandeputte has a Research Assistantship of the Fund for Scientific Research—Flanders, Belgium (F.W.O.—Vlaanderen).

References

1 L. J. Broadbelt and J. Pfaendtner, *AIChE J*., 2005, **51**, 2112–2121.
2 M. G. Evans and M. Polanyi, *Proc. R. Soc. London, Ser. A*, 1936, **154**, 1333–1360.
3 M. G. Evans and M. Polanyi, *Trans. Faraday Soc*., 1938, **34**, 11–29.
4 P. Blowers and R. Masel, *AIChE J*., 2000, **46**, 2041–2052.
5 W. H. Green, *Adv. Chem. Eng*., 2007, **32**, 1–50.
6 A. A. Zavitsas, *J. Am. Chem. Soc*., 1998, **120**, 6578–6586.
7 X. L. Ma and H. H. Schobert, *Ind. Eng. Chem. Res*., 2003, **42**, 1151–1161.
8 P. F. Su, L. C. Song, W. Wu, P. C. Hiberty and S. Shaik, *J. Am. Chem. Soc*., 2004, **126**, 13539–13549.
9 S. W. Benson and J. H. Buss, *J. Chem. Phys*., 1958, **29**, 546–561.
10 S. W. Benson, in *Thermochemical Kinetics*, John Wiley & Sons Ltd., New York, 1st edn, 1968.
11 P. A. Willems and G. F. Froment, *Ind. Eng. Chem. Res*., 1988, **27**, 1959–1966.
12 P. A. Willems and G. F. Froment, *Ind. Eng. Chem. Res*., 1988, **27**, 1966–1971.
13 R. Sumathi, H. H. Carstensen and W. H. Green, *J. Phys. Chem. A*, 2001, **105**, 6910–6925.
14 R. Sumathi, H. H. Carstensen and W. H. Green, *J. Phys. Chem. A*, 2001, **105**, 8969–8984.
15 R. Sumathi, H. H. Carstensen and W. H. Green, *J. Phys. Chem. A*, 2002, **106**, 5474–5489.
16 T. N. Truong, *J. Chem. Phys*., 2000, **113**, 4957–4964.
17 S. W. Zhang and T. N. Truong, *J. Phys. Chem. A*, 2003, **107**, 1138–1147.
18 N. Kungwan and T. N. Truong, *J. Phys. Chem. A*, 2005, **109**, 7742–7750.
19 M. Saeys, M. F. Reyniers, G. B. Marin, V. Van Speybroeck and M. Waroquier, *AIChE J*., 2004, **50**, 426–444.
20 M. Saeys, M. F. Reyniers, V. Van Speybroeck, M. Waroquier and G. B. Marin, *ChemPhysChem*, 2006, **7**, 188–199.
21 M. K. Sabbe, M. F. Reyniers, V. Van Speybroeck, M. Waroquier and G. B. Marin, *ChemPhysChem*, 2008, **9**, 124–140.
22 S. W. Benson, F. R. Cruickshank, D. M. Golden, G. R. Haugen, H. E. O'Neal, A. S. Rodgers, R. Shaw and R. Walsh, *Chem. Rev*., 1969, **69**, 279–324.
23 N. Cohen and S. W. Benson, *Chem. Rev*., 1993, **93**, 2419–2438.
24 J. W. Ochterski, G. A. Petersson and J. A. Montgomery, *J. Chem. Phys*., 1996, **104**, 2598–2619.
25 H. H. Carstensen and A. M. Dean, *J. Phys. Chem. A*, 2009, **113**, 367–380.
26 J. A. Montgomery, M. J. Frisch, J. W. Ochterski and G. A. Petersson, *J. Chem. Phys*., 1999, **110**, 2822–2827.
27 M. L. Coote, *J. Phys. Chem. A*, 2004, **108**, 3865–3872.

28 K. Hemelsoet, D. Moran, V. Van Speybroeck, M. Waroquier and L. Radom, *J. Phys. Chem. A*, 2006, **110**, 8942–8951.
29 J. Pfaendtner, X. R. Yu and L. J. Broadbelt, *J. Phys. Chem. A*, 2006, **110**, 10863–10871.
30 B. Temelso, C. D. Sherrill, R. C. Merkle and R. A. Freitas, *J. Phys. Chem. A*, 2006, **110**, 11160–11173.
31 A. G. Vandeputte, M. K. Sabbe, M. F. Reyniers, V. Van Speybroeck, M. Waroquier and G. B. Marin, *J. Phys. Chem. A*, 2007, **111**, 11771–11786.
32 C. Eckart, *Phys. Rev.*, 1930, **35**, 1303–1309.
33 K. J. Laidler, in *Chemical Kinetics*, Harper Collins, New York, 3rd edn, 1987.
34 *GAUSSIAN 03 (Revision B.03)*, Gaussian, Inc., Wallingford, CT, 2004.
35 E. L. I. Pollak and P. Pechukas, *J. Am. Chem. Soc.*, 1978, **100**, 2984–2991.
36 A. J. Karas, R. G. Gilbert and M. A. Collins, *Chem. Phys. Lett.*, 1992, **193**, 181–184.
37 T. N. Truong and D. G. Truhlar, *J. Chem. Phys.*, 1990, **93**, 1761–1769.
38 T. N. Truong, *J. Phys. Chem. B*, 1997, **101**, 2750–2752.
39 D. G. Truhlar and B. C. Garrett, *J. Phys. Chem. A*, 2003, **107**, 4006–4007.
40 V. Van Speybroeck, D. Van Neck, M. Waroquier, S. Wauters, M. Saeys and G. B. Marin, *J. Phys. Chem. A*, 2000, **104**, 10939–10950.
41 P. Vansteenkiste, V. Van Speybroeck, G. B. Marin and M. Waroquier, *J. Phys. Chem. A*, 2003, **107**, 3139–3145.
42 V. Van Speybroeck, P. Vansteenkiste, D. Van Neck and M. Waroquier, *Chem. Phys. Lett.*, 2005, **402**, 479–484.
43 P. Vansteenkiste, D. Van Neck, V. Van Speybroeck and M. Waroquier, *J. Chem. Phys.*, 2006, **124**, 044314.
44 M. K. Sabbe, A. G. Vandeputte, M. F. Reyniers, V. Van Speybroeck, M. Waroquier and G. B. Marin, *J. Phys. Chem. A*, 2007, **111**, 8416–8428.
45 D. R. Coulson, *J. Am. Chem. Soc.*, 1978, **100**, 2992–2996.
46 T. N. Truong, W. T. Duncan and M. Tirtowidjojo, *Phys. Chem. Chem. Phys.*, 1999, **1**, 1061–1065.
47 A. Violi, T. N. Truong and A. F. Sarofim, *J. Phys. Chem. A*, 2004, **108**, 4846–4852.
48 L. K. Huynh, S. Panasewicz, A. Ratkiewicz and T. N. Truong, *J. Phys. Chem. A*, 2007, **111**, 2156–2165.
49 Carstensen and Dean observed that the B3LYP-optimized transition-state structures, which is the CBS-QB3 built-in procedure, deviated significantly from the expected geometry for the several hydrogen abstractions such as the abstraction by a hydrogen radical from propene yielding an allyl radical. In this work however, the expected geometry was determined in which the breaking C–H bond is in overlap with the neighboring pi system. In contrast to the suspicion of Carstensen and Dean that the CBS-QB3 calculations might need to be replaced with more precise calculation methods, the CBS-QB3 geometry optimization seems to be reliable according to our calculations.
50 Y.-R. Luo, in *Handbook of Bond Dissociation Energies in Organic Compounds*, CRC Press, Boca Raton, 2003.
51 M. K. Sabbe, F. De Vleeschouwer, M. F. Reyniers, M. Waroquier and G. B. Marin, *J. Phys. Chem. A*, 2008, **112**, 12235–12251.
52 Chemical Kinetics Database, Standard Reference Database 17, Version 7.0 (Web Version), Release 1.3. http://kinetics.nist.gov/ 2005.
53 W. Tsang, *J. Phys. Chem. Ref. Data*, 1990, **19**, 1–68.
54 M. C. Paputa and S. J. W. Price, *Can. J. Chem.*, 1979, **57**, 3178–3181.
55 R. Louw, *Recueil*, 1971, **90**, 469.
56 H. X. Zhang, S. I. Ahonkhai and M. H. Back, *Can. J. Chem.*, 1989, **67**, 1541–1549.
57 D. G. L. James and E. W. R. Steacie, *Proc. R. Soc. London, Ser. A*, 1958, **244**, 289.
58 L. Szirovicza and F. Marta, *Int. J. Chem. Kinet.*, 1976, **8**, 897–910.
59 R. E. berkley, G. N. C. Woodall, O. P. Strausz and H. E. Gunning, *Can. J. Chem.*, 1969, **47**, 3305.
60 L. Seres, R. Fischer, K. Scherzer and M. Gorgenyi, *J. Chem. Soc., Faraday Trans.*, 1995, **91**, 1303–1312.
61 L. Szirovicza and F. Marta, *Magy. Kem. Foly.*, 1979, **85**, 369–373.
62 T. Kortvelyesi and L. Seres, *J. Chem. Soc., Faraday Trans.*, 1992, **88**, 2445–2450.
63 C. Richard and R. Martin, *Int. J. Chem. Kinet.*, 1985, **17**, 389–399.
64 M. C. Lin and M. H. Back, *Can. J. Chem.*, 1966, **44**, 2369.
65 C. Collongues, C. Richard and R. Martin, *Int. J. Chem. Kinet.*, 1983, **15**, 5–23.

